NASA TECHNICAL NOTE

NASA TN D-5338

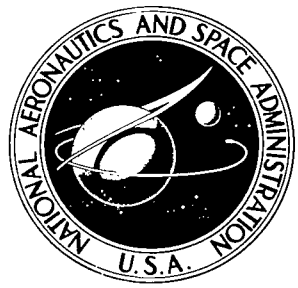

NASA TN D-5338

DYNAMIC RESPONSE OF A MACH 2.5 AXISYMMETRIC INLET WITH ENGINE OR COLD PIPE AND UTILIZING 60 PERCENT SUPERSONIC INTERNAL AREA CONTRACTION

by Joseph F. Wasserbauer

Lewis Research Center
Cleveland, Ohio

NATIONAL AERONAUTICS AND SPACE ADMINISTRATION • WASHINGTON, D. C. • JULY 1969

DYNAMIC RESPONSE OF A MACH 2.5 AXISYMMETRIC INLET WITH ENGINE OR COLD PIPE AND UTILIZING 60 PERCENT SUPERSONIC INTERNAL AREA CONTRACTION

By Joseph F. Wasserbauer

Lewis Research Center
Cleveland, Ohio

NATIONAL AERONAUTICS AND SPACE ADMINISTRATION

For sale by the Clearinghouse for Federal Scientific and Technical Information
Springfield, Virginia 22151 – CFSTI price $3.00

ABSTRACT

The inlet was subjected to sinusoidal bypass area disturbances with frequencies up to 240 hertz and to sinusoidal external disturbances with frequencies up to 15 hertz. Dynamic response data are presented for terminal shock position and selected static pressures throughout the inlet. These results were obtained for the inlet coupled to either an engine or to a cold-pipe configuration. The effect of varying the cold-pipe length and throat bleed configuration are also presented. The dynamic response of the inlet to bypass area disturbances exhibited resonant conditions. The effect of an engine could be simulated with a cold pipe of appropriate length.

DYNAMIC RESPONSE OF A MACH 2.5 AXISYMMETRIC INLET WITH ENGINE OR COLD PIPE AND UTILIZING 60 PERCENT SUPERSONIC INTERNAL AREA CONTRACTION

by Joseph F. Wasserbauer

Lewis Research Center

SUMMARY

A study has been made to experimentally determine the dynamic response of a supersonic mixed-compression inlet designed for operation at Mach 2.5. The inlet was coupled either to a short or long cold pipe or to an operating turbojet engine. Dynamic response of the terminal shock and of selected static pressures within the inlet were determined for configurations with and without bleed in the region of shock motion. The inlet-cold-pipe and inlet-engine configurations were subjected to symmetrical sinusoidal bypass area disturbances at frequencies up to 140 hertz and to an unsymmetrical disturbance at frequencies up to 240 hertz. A sinusoidal external disturbance provided flow perturbations at frequencies up to 15 hertz.

The dynamic response of the inlet exhibited a resonance at 55 hertz and repeated resonances at higher frequencies for the inlet configurations utilizing throat bleed. Little or no change in the primary resonant frequency was observed when the cold-pipe length was changed or when the engine was coupled to the inlet. The amplitude of the response was more attenuated, however, with the largest internal volume. The inlet dynamic response was observed to be similar for the inlet-engine configuration and the cold-pipe configuration with the choke point near the engine-face station. Sealing the downstream throat bleed increased the sensitivity of the terminal shock to internal disturbances and reduced the frequency at which the primary resonance occurred. The dynamic response of the inlet to an external disturbance exhibited a lead characteristic at about 15 hertz.

INTRODUCTION

As recently as three years ago, experimental data for inlet dynamics were limited to internal disturbance frequencies less than 50 hertz. In reference 1, this range was extended to 200 hertz. These experimental results were the first to exhibit resonant conditions in the dynamic response of the inlet at frequencies greater than 50 hertz. These resonances were later predicted by the analysis presented in reference 2. However, the inlet of reference 1 was connected to a cold-pipe configuration with a large volume between the diffuser exit station and the choked exit plug and provided no internal volume variation. In order to obtain a more comprehensive understanding of an inlet's dynamic response, it is necessary to extend the previous work to a configuration more representative of current supersonic propulsion systems. Therefore, it is of interest to obtain the dynamic response of an inlet coupled to an operating turbojet engine as well as an inlet coupled to a cold pipe with internal volume variations.

A test of this nature was subsequently conducted in the Lewis 10- by 10-Foot Supersonic Wind Tunnel. These configurations were subjected to symmetrical and unsymmetrical internal disturbances by varying the inlet's overboard bypass-exit area at frequencies up to 240 hertz and also to an external disturbance at frequencies up to 15 hertz. Preliminary results are presented in reference 3. As in reference 1, a bypass-exit area variation was used as the internal disturbance since (1) it is well defined, (2) real disturbance might be of this nature, and (3) control loops are closed through bypass area devices as in reference 4. Data were also obtained for two inlet performance bleed configurations to determine the effect of performance bleed on the inlet dynamic response. Some comparisons of the experimental data are made with the analysis presented in references 2 and 3.

SYMBOLS

A	flow area
A_i	inlet capture area, 0.1758 m^2
A_{by}	bypass door exit area
M	Mach number
m/m_0	mass flow ratio
P	total pressure, N/m^2
p	static pressure, N/m^2
R	radius

R_c	cowl lip radius, 0.2366 m
Re	Reynolds number
r	radius
T	total temperature, K
w	air flow, kg/sec
$w\sqrt{\theta}/\delta$	engine corrected air flow
x	axial distance from spike tip, m
γ	ratio of specific heats
Δ	increment
δ	$P/10.131\times10^4$ N/m^2
θ	T/288.2 K
φ	gust plate angle of attack, deg

Subscripts:

x	local
0	free stream

APPARATUS AND PROCEDURE

Model

The experimental investigation was conducted in the Lewis 10- by 10-Foot Supersonci Wind Tunnel. Table I lists the average free-stream conditions used during the investigation. The heated tunnel conditions for all Mach numbers are given in reference 5.

TABLE I. - AVERAGE FREE-STREAM CONDITIONS

Tunnel condition	Free-stream conditions			Ratio of specific heats, γ	Reynolds number per foot, Re	Tunnel cycle
	Mach number	Total pressure, P_0, N/m^2	Total temperature, T_0, K			
Unheated	2.497	8.90×10^4	318	1.400	8.10×10^6	Aerodynamic
Unheated	2.497	9.95	343	1.400	8.10	Propulsion
Heated	2.462	10.32	390	1.394	7.10	Propulsion

The inlet was an axisymmetric, mixed-compression type designed for Mach 2.5 operation with 60 percent of the total supersonic area contraction occurring internally. An isometric view of the inlet is shown in figure 1. The inlet had a cowl-lip diameter of 0.465 meter, and provisions were made for boundary-layer bleed on the cowl and centerbody in the inlet throat region. The relative locations of the cowl performance bleed exits and the overboard and ejector bypass exits are shown in figure 1. Vortex generators were used on the centerbody of the inlet. The aft portion of the subsonic diffuser was compartmented back to the engine-face station by three hollow centerbody support struts. The centerbody performance bleed flow was ducted to the free stream through two of these support struts. Just ahead of the engine face in each compartmented section of the diffuser, the bypass entrance and plenum were divided into separate equal sections by a cowl rib. Each of the six separate sections contained an overboard bypass-door unit and an ejector bypass-exit valve. The steady-state performance characteristics of this inlet are reported in references 6 to 9.

Three diffuser terminations were studied during the investigation and are shown schematically in figure 2. The inlet was terminated at the diffuser exit by (1) a long cold-flow pipe with the internal flow choked at the exit plug, located 236 centimeters from the engine-face station (see figs. 5 and 9), (2) a choke plate positioned 11.43 centimeters downstream of the engine-face station, and (3) a J85-GE-13 turbojet engine (the inlet guide vanes are 5.7 cm from the engine-face station). The corrected airflow requirement for military operation of the engine was 15.38 kilograms per second at a temperature of 390 K. Engine operation with this inlet is discussed in detail in reference 9. Details of the choke plate are shown in figure 3. Its total flow area is 653.07 square centimeters. Assuming a 98-percent flow coefficient, this area is 97.5 percent of the area needed to match the engine corrected airflow requirement.

Two inlet throat bleed patterns were used and are shown in figure 4. The basic bleed configuration used in the test is configuration II (configuration II ND', ref. 7). Configuration I was used to determine the effect of sealing the bleed, in the region of terminal shock motion, on the terminal shock dynamic response. Selection of the bleed configurations is based on the results of references 6 and 7. However, for the bleed configuration I (configuration I of ref. 7) the inlet did not have the vortex generators installed on the centerbody in reference 7.

Some of the design details are summarized in figures 5 and 6. Figure 5(a) presents the inlet flow area variation for the design Mach number of 2.5. Shown in the figure are the model choke points for the long and short cold pipe and also the location of the engine face. Indicated in the figure is the location of the entrance to the bypass plenum at which point the internal flow disturbance generated by the bypass doors or rotary valve was transmitted to the main duct flow. Figure 5(b) presents the total cross-sectional area variation of the six bypass cavities. Figure 6(a) presents the theoretical

flow conditions and inlet dimensions for the cowl and centerbody surfaces at the design Mach number of 2.5. The experimental performance of configuration II is shown in figure 6(b). The inlet characteristics were obtained either by maintaining constant bypass position and varying plug position or by maintaining constant simulated engine corrected airflow with the plug and varying bypass flow through those doors not being used as a disturbance device. The inlet operating conditions for each dynamic response are indicated in the appropriate figures. The dynamic data for the internal disturbances with the long-cold-pipe and choke-plate terminations were obtained with the inlet operating at or near the engine match corrected airflow line of 15.83 kilograms per second.

All dynamic data were taken with the terminal shock positioned about 6 centimeters downstream of the inlet's geometric throat ($m/m_0 = 0.905$, $P/P_0 = 0.92$, fig. 6(b)). Figure 6(c) shows the steady-state internal-cowl pressure distributions for three bypass-door positions which provided the midposition and end points of shock excursion during dynamic operation. Figure 6(d) shows the effect of throat bleed on shock position in the inlet throat produced by varying bypass-door exit area. With the shock positioned on the downstream bleed zones of the cowl and centerbody, the shock motion is greatly attenuated with open bleed. Some nonlinearity was experienced for shock excursions beyond $x/R_c = 3.8$ when the downstream bleed was operating.

Disturbance Devices

Internal and external disturbance devices were used to perturb the inlet flow. The internal disturbance devices were the overboard bypass doors of the inlet and a rotary bypass valve. One of the inlet's six overboard bypass doors is shown in figure 7(a). Each door was independently controlled by means of an individual electrohydraulic servomechanism which is described in reference 10. The overboard bypass door servos had a constant amplitude response to frequencies of 100 hertz when operated sinusodially with an incremental exit area amplitude of 16.13 square centimeters per door, peak to peak. From 100- to 140-hertz, attenuation of the amplitude response was experienced. Three symmetrically located overboard-bypass-door servos were driven by a common command signal to produce a symmetrical internal disturbance. Typical incremental area variation per door, peak to peak, for the symmetrical distrubance was 24.2 square centimeters. One overboard bypass door that was located in line with the dynamic instrumentation was operated sinusoidally to produce an unsymmetrical internal disturbance. The bypass-door oscillations were limited to 100 hertz for one test series because of temporary stress limitations in the door linkages. A redesign of the door linkage permitted oscillation of the bypass doors to 140 hertz for the remaining tests.

The frequency range of the unsymmetrical disturbance was extended by replacing one overboard bypass door (the door that was in line with the dynamic instrumentation) with a rotary valve, which operated at frequencies up to 240 hertz. The exit area of the rotary valve was designed to vary in a sinusoidal manner. Details of the rotary valve assembly and exit ports are exhibited in figures 7(b) and (c). The total incremental exit area variation of the rotary valve was 20.5 square centimeters. A complete description of the design and operation of the rotary valve is presented in reference 1. Two modifications were made to the rotary valve for the present investigation: The rotating cam had four lobes rather than the two lobes of reference 1, and a magnetic pickup provided a pulse signal that was used to monitor valve frequency and established a reference to determine phase shift.

The external disturbance was generated by a large trapezoidal gust plate mounted in the tunnel just upstream of the inlet as in reference 1 and is schematically shown in figure 2(a). The gust plate presents a uniform two-dimensional flow disturbance to the inlet. Oscillation of the gust plate changes the local inlet Mach number and angle of attack. Three modes of gust plate operation were used with the gust plate sinusodially operated through one degree of arc at frequencies up to 15 hertz. The three modes of operation for the gust plate were that (1) the gust plate oscillated from 0° to -1° angle of attack (increasing inlet Mach number), (2) the gust plate oscillated at $\pm 1/2^{\circ}$ about 0° angle of attack (increasing and decreasing inlet Mach number), and (3) the gust plate oscillated from 0° to 1° angle of attack (decreasing inlet Mach number). The gust-plate deflection angles were so slight that there was a negligible change in the local total pressure ahead of the inlet.

Figure 8 shows the inlet model installed in the Lewis 10- by 10-Foot Supersonic Wind Tunnel and indicates its relative size. The disturbance devices and their location with respect to the inlet model are also indicated. The rotary valve was removed when the bypass doors were used as the internal flow disturbance.

Instrumentation and Data Reduction

The response of the pressures in the diffuser to the flow perturbations was sensed with strain-gage pressure transducers and recorded on magnetic tape. The coupling tube length for each transducer was kept short (about 3 to 4 cm long). Each tube-transducer assembly was calibrated in frequency response so that later corrections could be made to the dynamic response data. The tube-transducer assemblies had resonant frequencies from about 350 to 600 hertz. The locations of the dynamic instrumentations are shown in figure 9. All static-pressure taps were located in line 30° from the top centerline on the inlet cowl (clockwise looking upstream) except for the engine-face

static-pressure tap, which was located on the centerbody. However, this tap was located at the same angular position as the cowl taps. An enlarged view of the inlet terminal shock position instrumentation is shown in figures 4 and 10. The instrumentation is staggered about the 30° centerline (view A-A, fig. 10) to minimize the effect of the cowl bleed orifices on the measured pressure and to provide room for mounting the transducers.

Shock position dynamics were obtained by first noting the shock crossing times from the analog signal of each transducer as the terminal shock traversed the inlet throat region in a sinusoidal manner. The times of shock crossing for each transducer were combined with the transducer locations to obtain a sinusoidal curve fit by the method of least squares, which provided the amplitude and phase shift of the shock position. This method of data reduction for the shock position dynamics is described completely in reference 1. The technique is limited to frequencies below 100 hertz because of attenuation in the transducer signals at higher frequencies.

Before dynamic data were recorded, the terminal shock mean position was set at the midpoint of the eight throat transducers. The incremental change in the shock position was determined by oscillating the disturbance at 1 hertz and then determining the amplitude of shock excursion by the method of least squares. As a check on the shock position amplitude at 1 hertz, steady-state data were recorded with the disturbance device set at its midposition and at its excursion end points (fig. 6(c)). The shock position amplitudes obtained by the two methods showed good agreement.

In addition to the check on shock position amplitude, the steady-state data for the bypass-door excursion end points determined the incremental change in pressure throughout the inlet as well as the amount of bypass flow necessary to cause this change. These data are presented in the respective figures as ratios of the increment in shock position or pressure to the increment in bypass exit airflows $\Delta x/\Delta w$ and $\Delta p/\Delta w$, respectively. The steady-state data for the external disturbance determined the increment in shock position and pressure to the increment in gust-plate angle of attack $\Delta x/\Delta\varphi$ and $\Delta p/\Delta\varphi$, respectively.

All the dynamic data were recorded on analog tape. With the exception of the eight throat transducers, the pressure data were digitized and then processed through a digital computer program to give phase shift and amplitude ratio. All data were corrected to compensate for the dynamics of the disturbance devices and tube-transducer assemblies. For the case of the rotary valve, only the dynamics of the tube-transducer assembly had to be considered since the variation of the exit area remained constant over the entire frequency range.

All data presented in the succeeding figures are in terms of amplitude ratio and phase shift. The amplitude ratio is defined as the signal amplitude at the test frequency divided by the amplitude at zero frequency. The amplitude for zero frequency was as-

sumed to be the same as the amplitude recorded at a frequency of 1 hertz or less for the shock position and the static-pressure responses.

RESULTS AND DISCUSSION

Symmetrical Internal Disturbance

The dynamic response of shock position and inlet static pressures to a symmetrical sinusoidal exit area variation of the three overboard bypass doors is presented in figure 11 for inlet configuration II terminated with the long cold pipe. The pressure data are not presented beyond 100 hertz for this configuration because of the stress limitations in the bypass-door linkages. The data of figure 11 indicate an initial large reduction in amplitude ratio as the disturbance frequency increased to about 25 or 30 hertz. This behavior corresponds to the first-order lag associated with the large internal volume. For the shock position dynamics, a resonance is observed at about 55 hertz with a second resonance indicated above 100 hertz (fig. 11(a)). Repeated resonances suggest that the system dynamics could be represented by a distributed parameter system. Reference 2 describes an analysis that subdivides the subsonic duct into constant area sections which are represented by one-dimensional wave equations. The movable terminal shock and the choked exit station serve as the boundary conditions. The analysis leads to closed-form solutions for shock position and pressure frequency response. Comparison of the shock position data of figure 11(a) and the analysis of reference 2 was presented in reference 3 with an additional consideration in the analysis for the loss in weight flow in the throat due to performance bleed. Good agreement was obtained in reference 3 between the experimental data and the analysis when the analytical parameter defining the throat geometry with bleed effects was empirically determined.

The response of static pressures at various locations throughout the inlet to bypass-door area variation is presented in figures 11(b) to (e). The resonance at 55 hertz and the indications of repeated resonances at the higher frequencies are also evident in these internal duct dynamics back to the engine face. An exception to this trend is the response of the cold-pipe static pressure located further aft (see fig. 5(a)) which exhibits a damped resonance at about 40 hertz (fig. 11(f)). The response of the static pressure near the entrance to the bypass cavity (fig. 11(c)) and that in the bypass plenum (fig. 11(d)) appear to be identical for this configuration. Therefore, the bypass cavity appears to be well coupled to the main diffuser and exhibits no unique dynamics of its own.

A rather unusual response was observed for the engine-face static-pressure for this long-cold-pipe configuration (fig. 11(e)). More distinct nodal points and resonances

are exhibited for the amplitude ratio than shown for the other static pressures. The response in phase shift observed over the frequency range shows a sharp reversal from a phase lag to a phase lead at the nodal point of 30 hertz. This is followed by decreasing phase shift until the next nodal point at 90 hertz where another sharp reversal in phase shift is noted. Since only the long-cold-pipe configuration exhibited this response at the engine face, there may be an interaction associated with the cold-pipe resonance at 40 hertz (exhibited by the cold-pipe static pressure) and the 55-hertz resonance (apparent in the response data upstream of the engine face).

The dynamic response of the inlet to a symmetrical sinusoidal exit area variation of the bypass doors for bleed configuration II with the choke plate installed at the engine face is presented in figure 12. The initial reduction in amplitude ratio is much less as a result of the reduced volume. A resonance is still apparent at 50 to 55 hertz for the response of the shock position, the throat-exit static pressure, and the engine-face static pressure (figs. 12(a), (b), and (e), respectively). The response of the static pressure before and in the bypass plenum cavity does not exhibit an obvious resonant frequency but does have a flat amplitude ratio response from about 40 to 100 hertz (figs. 12(c) and (d)). The analytical results of reference 3 are compared with experimental data of shock position and throat-exit static pressure (figs. 12(a) and (b)). In both responses, the phase agreement is good, but, although the analytical results exhibit a plateau in the amplitude ratio responses, they fail to exhibit the distinct resonance of the test data. The theory may be inadequate in this regard since it neglects the bypass cavity volume and only simulated throat bleed effects in an approximate manner.

The response for the inlet configuration II, with the choke plate and with the tunnel total temperature increased from 317 to 388 K by means of the tunnel heater, is presented in figure 13. The change in the dynamic response of the inlet was expected to be small since, in general, a change in the resonant frequency due to temperature change is proportional to the square root of the temperature ratio, and the change in phase shift due to dead time is inversely proportional to the square root of the temperature ratio. Based on these considerations, the resonant frequency should have increased about 10 percent with a corresponding reduction of about 10 percent in phase shift at the resonant condition. Comparison of figures 12 and 13 indicates that these small changes in the dynamic response were probably realized. The data for the response of the static pressures before and in the bypass plenum cavity were not obtained for this test.

The dynamic response of inlet configuration II to a symmetrical internal disturbance for the inlet coupled to the J85-GE-13 turbojet engine at tunnel total temperatures of 344 K (unheated) and of 390 K (heated) is presented in figures 14 and 15, respectively. For the high-temperature condition, the engine was operated at 98 percent of rated mechanical speed or 85 percent of corrected speed. For the low-temperature condition, the engine was operated at 90 percent of rated mechanical speed or 81 percent of cor-

rected speed. For this temperature increase, the compressor pressure ratio was increased from 3.4 to 4.0, and the power lever angle was increased from 39° to 63°. Therefore, when the comparisons are made for the two test conditions, the effect of the change in free-stream total temperature and engine operating conditions are made simultaneously. The response in shock position again exhibits the resonance at about 55 hertz, and little or no difference is noted when the free-stream total temperature was increased (figs. 14(a) and 15(a)). The response of the throat-exit static pressure also exhibits little change (figs. 14(b) and 15(b)). The response of the static pressure before the bypass plenum cavity shows no noticeable resonance over the disturbance frequency range and little difference in response between the low- and high-temperature conditions, except at the higher frequencies (figs. 14(c) and 15(c)). The dynamic response of the static pressure in the bypass cavity (figs. 14(d) and 15(d)) indicates that a resonance appears at about 80 to 85 hertz. This resonance was more pronounced when the free-stream total temperature was increased. The static-pressure response at the engine face shows little difference for the free-stream total temperature change except at the higher frequencies (figs. 14(e) and 15(e)). Although there are changes in the response of the static pressure at different locations in the inlet, the differences in response at a given inlet location due to changes in free-stream total temperature and engine operating conditions appear to be small.

Figure 16 presents a summary comparison of the inlet dynamic response obtained from a symmetrical internal disturbance for configuration II with the inlet terminated with the long cold pipe, the choke plate, and a turbojet engine. Consideration of the shock position dynamics (fig. 16(a)) shows that changing the cold-pipe length or coupling the inlet to a turbojet engine did not change the frequency of the primary resonance.

The effect of volume is indicated by noting the rapid decrease in the amplitude ratio for the long cold pipe compared with a gradual decrease for the other two inlet terminations. First-order lumped parameter analysis such as that of reference 11 can be used to predict the data to resonances such as those observed in this test. The analysis presented in reference 2 predicts these resonances and avoids the complexity of the method of characteristics.

The response in static pressures throughout the inlet with the long-cold-pipe termination also differed substantially from those of the other configurations (figs. 16(b) to (d)). A comparison of the engine and choke-plate responses shows that the engine curves, in general, drop off faster in amplitude ratio and show more pronounced resonance, which indicates that the effective volume of the inlet-engine system was somewhat greater than that of the choke-plate configuration. In figure 16(e), an exception is noted which shows that the response for the inlet-engine configuration at this station is greater in magnitude than the choke-plate configuration. The preceeding comparisons would suggest that, in future tests of the inlet shock response to an internal symmetrical dis-

turbance, the effect of an engine can be simulated by positioning a choke plate a short distance downstream of the compressor face.

The effect of sealing the downstream throat performance bleed of the inlet (configuration I with the engine installed) is presented in figure 17 for the response of the shock position and inlet static pressures to a symmetrical internal disturbance. The amplitude of the sinusoidal variations of the bypass-door exit area was reduced for this test series since small variations of the inlet back pressure resulted in large excursions of the terminal shock in the inlet throat for this bleed configuration. The ratio of the change in shock position to a change in bypass-door exit area for inlet configuration I (fig. 17) was about 4.3 times that of configuration II (fig. 14) at the reference disturbance frequency of 1 hertz.

A comparison of the dynamic response of the inlet shock position and static pressures for the performance bleed configurations I and II is shown in figure 18. The comparisons are made for the inlet terminated with the turbojet engine. The resonant frequency was reduced from 55 to about 50 or 45 hertz for both the shock position and throat-exit static-pressure responses when the downstream throat bleed was sealed (figs. 18(a) and (b)). Small differences in phase shift were noted for these two responses. Comparisons of the response of the static pressures at the other locations in the inlet also exhibits the reduction in resonant frequency when the downstream throat bleed is sealed (figs. 18(c) to (e)).

Unsymmetrical Internal Disturbance

Generally, an unsymmetrical internal disturbance would be more likely to occur in an inlet than a symmetrical disturbance. To explore any differences that may occur, an additional series of experimental data are presented for inlet configurations I and II terminated with the engine and also for configuration I terminated with the long and short cold pipes. For the inlet terminated with the engine, one bypass door was used as the disturbance, while the rotary valve was used with the long and short cold pipes.

Comparisons with previous data of the shock position and throat-exit static-pressure dynamics for both inlet configurations (figs. 19(a) and (b), respectively, for configuration II and figs. 20(a) and (b), respectively, for configuration I) indicate that the trends are similar to the response for a symmetrical disturbance (figs. 18(a) and (b)). However, the response of the static pressures in the portion of the diffuser segmented by struts shows a different dynamics than was observed for the symmetrical disturbance. As indicated earlier in the section APPARATUS AND PROCEDURE, the dynamic instrumentation is located in line with the unsymmetrical disturbance 30° from the top centerline. The other two segmented portions of the diffuser were not instrumented. For config-

uration II, these static pressures showed a rather moderate decrease in the response of the amplitude ratio and a slight rise in the amplitude ratio at about 85 hertz (figs. 19(c) to (e)). For configuration I, the same trends are observed but for an extended frequency range; the amplitude ratio shows an increasing trend to at least 140 hertz. The most pronounced effect is seen in response of the static pressure at the engine-face station (fig. 20(e)). Here, the amplitude ratio at 140 hertz is greater than 1.0. This would indicate that, although the response of the shock position and throat-exit static pressures are similar for a symmetrical and unsymmetrical disturbance, the dynamics for the two types of distrubances can be quite different in a segmented portion of an inlet. A static pressure selected for inlet control should be affected in the same way by both symmetrical or unsymmetrical disturbances. Such a control signal could be provided by the throat-exit static-pressure tap. Reference 4 presents the results of a high-performance bypass control system for this inlet using the throat-exit static-pressure signal as the controlling signal.

The disturbance frequency range was extended up to 240 hertz with the rotary valve for inlet configuration I terminated with the long cold pipe and choke plate. The rotary valve was not used when the inlet-engine configurations were tested. The response to the rotary valve of configuration I with the choke-plate termination is presented in figure 21. The data of figure 21(c) terminate at 130 hertz due to electronic difficulties with this channel. In general, the responses of the choke position and the diffuser static pressures for this inlet configuration termination are similar to that of the responses in figure 20. Here again, the experimental data show that the inlet dynamics with the engine termination can be approximated by using a choke plate near the engine-face station. The response of the engine-face static-pressure (fig. 21(e)) shows that a minimum in the amplitude ratio is reached at 50 hertz and that a large resonance occurs at about 160 hertz. The magnitude of the amplitude ratio at this resonance is greater than the reference amplitude at 1 hertz.

The response of configuration I terminated with the long pipe is presented in figure 22. The first resonant condition for shock position and all the static-pressure responses appears at about 45 hertz. A characteristic of the long-cold-pipe termination for either configuration I or II and for either a symmetrical or unsymmetrical disturbance appears to be that the first resonance is observed at the same frequency for the shock position and static-pressure responses. Comparison of the throat-exit static-pressure responses of figures 21(b) and 22(b) shows that the first resonant condition at 45 hertz has been damped for the choke-plate termination and that the resonant condition at about 110 hertz is eliminated. Comparison of the phase shift for these two inlet terminations shows that the response in phase shift is not the same in the vicinity of 100 hertz. The resonance at 160 hertz apperas in the response for both inlet terminations. Comparison of the responses of the static pressures in the vicinity of the bypass

cavity shows that the resonance conditions appear at about the same frequency (figs. 21(c) and (d) and figs. 22(c) and (d)). Figure 22(e) shows that the first resonance at 45 hertz for the engine-face static-pressure response is about one-half the magnitude of the resonance observed at 160 hertz. Comparison of the response of figure 22(e) to that of figure 21(e) shows that terminating the inlet with the choke plate results in eliminating or at least damping the resonance at 45 hertz and amplifying the resonance at 160 hertz by about 1.5 times. A possible reason for the difference in the two responses is that this portion of the inlet is segmented and that the varied paths of the pressure waves are different for the choke-plate and long-cold-pipe terminations.

Shock Position Dynamics - Inlet Unstart Method

The inlet unstart method of reference 1 was used to obtain a qualitative response of shock position dynamics. Determination of the shock position dynamics from shock crossing times and least squares method is limited to frequencies of about 100 hertz. For qualitative data on shock position dynamics beyond a frequency of 100 hertz, the inlet unstart method was used. A limitation of this method is that it provides dynamics of the terminal shock at only the limit of the inlet's stable range. The position of the terminal shock at unstart is well ahead of the throat and is located on the forward bleed of the cowl and centerbody. At this position, the terminal shock structure is fairly complex, but just before unstart, it is compressed into a plane wave as reported in reference 5. For this test, the model exit plug was fixed and the inlet unstarted at each of the test frequencies with one of the bypass doors. The rotary valve was used as the disturbing device. It is not certain that the terminal shock position was a linear function of the choked area of the bypass door or rotary valve when the normal shock was moved ahead of the inlet throat. Therefore, it is assumed that the shock position amplitude is only proportional to the bypass-door position. The rotary valve is set at the desired frequency, and then the inlet is unstarted with the bypass door. Then, an equivalent terminal shock oscillation amplitude ratio can be obtained from the unstart bypass-door position at each valve frequency.

In this method, the terminal shock does not oscillate about the same mean position when the amplitude is determined at different valve frequencies, and no phase information is obtained. However, as long as the relation between shock and bypass-door positions is valid, the method provides easily reduced data. In addition, the method has no characteristics that would impose a frequency limit on its use.

Unstart data were obtained for the two bleed configurations with the inlet terminated by the long cold pipe. Since the location of the shock position at unstart is on the bleed upstream of the geometric throat, the shock motion presented in figure 6(d) is no longer valid. Therefore, any effect on the inlet dynamics due to sealing downstream throat

bleed would be minimized. Resonant conditions appear at 60, 120, and about 200 hertz for configurations I and II (figs. 23(a) and (b)). Little difference is noted between the two responses.

Comparison of figure 23(a) with figure 11(a) shows that the primary resonant frequency has increased from 55 to 60 hertz when using the unstart method. In addition, the magnitude of the amplitude ratio at the first resonant condition is about 1.0 for the unstart method and only 0.55 when the dynamics were obtained in the previous manner using multiple transducers.

External Disturbance

The gust plate produced simultaneous changes in the free-stream Mach number and flow angle of attack in the flow field ahead of the inlet. The flow is perturbed in both the supersonic and subsonic portions of the duct. The manner in which the inlet was perturbed was (1) decreasing the Mach number ahead of the inlet (gust plate oscillating from 0° to 1° angle of attack), (2) increasing and decreasing Mach number (gust plate oscillating $\pm 1/2^{\circ}$ about 0° angle of attack), and (3) increasing Mach number (gust plate oscillating from 0° to -1° angle of attack).

External perturbations to an inlet are of interest since they may also be a cause of inlet unstart. Among the many reasons that could cause the forward motion of the terminal shock are (1) the reduction in the free-stream Mach number, which results in a decrease of the supersonic throat Mach number, an increase in the throat pressure recovery, and an increased corrected airflow, and (2) the change in angle of attack of this flow field when the gust plate was oscillated. This was verified from steady-state data by the increase in inlet pressure recovery when the gust plate was positioned from 0° to 1° angle of attack and also from the throat static transducers which indicated a forward motion of the terminal shock. By increasing Mach number ahead of the inlet (gust-plate motion from 0° to -1°), the terminal shock moves downstream or to a supercritical operating position. This also can be an undesirable occurrence since the increase in inlet distortion resulting from the supercritical operation could preciptate an engine stall. For all modes of gust-plate oscillation, the terminal shock moved in an asymmetrical manner in the inlet throat because operation at angle of attack causes its shock structure to become asymmetric. The response of shock position and the inlet static pressures to an external disturbance for inlet configuration II terminated with the turbojet engine are presented in figure 24. Before dynamic data were taken, the terminal shock was positioned at the midpoint of the throat transducers when the gust plate was positioned at 0°, $1/2^{\circ}$, and $-1/2^{\circ}$ for the various gust-plate oscillation modes. An increase in the amplitude of shock excursion (fig. 24(a)) was observed when the fre-

quency was increased from 1 to 15 hertz for a decreasing inlet Mach number ($\Delta\varphi = 0^{\circ}$ to 1°) and also for an increasing inlet Mach number ($\Delta\varphi = 0^{\circ}$ to -1°). When the gust plate was oscillated about its midposition ($\Delta\varphi = \pm 1/2^{\circ}$), a reduction in shock excursion was observed until about 6 hertz, then an increasing amplitude of shock excursion was experienced up to 15 hertz. As the gust-plate oscillation mode was changed from decreasing inlet Mach number to increasing inlet Mach number, the phase shift was increased from about -2° to -11° at 1 hertz and from about -90° to -130° at 15 hertz, respectively. This may result from the asymmetrical movement of the shock in the inlet throat for the various gust-plate oscillation modes.

The experimental trends presented in figure 24(b) for the throat-exit static pressure suggest a possible resonance in the amplitude ratio response beyond a disturbance frequency of 15 hertz. Little variation is noted in the amplitude ratio response for the three modes of gust-plate oscillations. The trends observed in the phase shift for shock position dynamics of figure 24(a) are also exhibited in the throat-exit static-pressure data of figure 24(b). However, the magnitude of the phase shift is not as great as that observed in the previous figure.

Figures 24(c) and (d) show responses of the static pressures near and in the bypass cavity. The response of the two are similar with a gradual reduction in the amplitude ratio to a frequency of 15 hertz. The phase shift for both responses had absolute values less than 50°. The phase for the gust-plate mode of 0° to -1° shows a lead characteristic from about 10 to 15 hertz. Again, this would suggest a possible resonance above 15 hertz.

The response of a static pressure at the engine face shows that the amplitude ratio exhibits little or no reduction in magnitude to about 10 hertz. A lead effect is indicated from 10 to 15 hertz by the magnitude of the amplitude ratio becoming greater than 1.0 at 15 hertz. The response in phase shift for all three modes of gust-plate oscillation for the static pressure at the engine face never has an absolute value greater than 30°.

The response of shock position and the inlet static pressures to an external disturbance for inlet configuration I terminated with the turbojet engine are presented in figure 25. In general, for the frequency range of the gust plate, the dynamics of the inlet for configuration II are the same as configuration I with a few exceptions in the shock position and in the static pressures before and in the bypass cavity.

The response of inlet configuration I to an external disturbance for the inlet terminated with the cold pipe is presented in figure 26. Comparisons of the respective responsed in figure 26 with those of figure 25 show that the effect of the additional volume of the cold pipe caused a general reduction in magnitude of the amplitude ratio and an increase in the absolute values of phase shift.

CONCLUSIONS

A mixed-compression inlet designed for Mach 2.5 was dynamically tested with both internal and external disturbances. The inlet was coupled to short- and long-cold-pipe configurations and also to an operating turbojet engine. These configurations were subjected to symmetrical internal disturbances at frequencies up to 140 hertz and to unsymmetrical internal disturbances at frequencies up to 240 hertz. The external disturbance provided flow perturbations at frequencies up to 15 hertz. Dynamic responses of both the terminal shock and the static pressures at various stations throughout the model were measured. The following results were obtained:

1. A resonance was observed at 55 hertz and repeated resonances occurred at higher frequencies for the shock position and diffuser static pressure responses for configurations utilizing throat bleed. Little change in the primary resonant frequency was observed when the internal flow choke points were changed or when the engine was coupled to the inlet.

2. The dynamic responses of the shock position and static pressures were observed to be similar for the inlet-engine configuration and the cold-pipe configuration with a choke plate installed near the engine-face station.

3. Sealing the downstream throat bleed increased the terminal shock sensitivity to downstream disturbances and reduced the frequency at which the primary resonance occurred.

4. With the unsymmetrical internal disturbance, the primary resonance is the predominant resonance for the shock position and throat-exit static-pressure responses, but the responses for the downstream static pressures exhibit a larger magnitude resonance at the second resonant frequency.

5. Some of the dynamic responses of the inlet to an external disturbance exhibit a lead characteristic in the amplitude ratio for the shock position dynamics at frequencies near 15 hertz.

Lewis Research Center,
National Aeronautics and Space Administration,
Cleveland, Ohio, March 18, 1969,
126-15-02-11-22.

REFERENCES

1. Wasserbauer, Joseph F.; and Whipple, Daniel L.: Experimental Investigation of the Dynamic Response of a Supersonic Inlet to External and Internal Disturbances. NASA TM X-1648, 1968.

2. Willoh, Ross G.: A Mathematical Analysis of Supersonic Inlet Dynamics. NASA TN D-4969, 1968.

3. Wasserbauer, Joseph F.; and Willoh, Ross G.: Experimental and Analytical Investigation of the Dynamic Response of a Supersonic Mixed-Compression Inlet. Paper 68-651, AIAA, June 1968.

4. Crosby, Michael J.; Neiner, George H.; and Cole, Gary L.: High Performance Bypass Control for Mixed-Compression Inlets. Paper 68-652, AIAA, June 1968.

5. Cubbison, Robert W.; and Meleason, Edward T.: Water Condensation Effects of Heated Vitiated Air on Flow in a Large Supersonic Wind Tunnel. NASA TM X-1636, 1968.

6. Cubbison, Robert W.; Meleason, Edward T.; and Johnson, David F.: Effect of Porous Bleed in a High-Performance, Axisymmetric, Mixed-Compression Inlet at Mach 2.50. NASA TM X-1692, 1968.

7. Cubbison, R. W.; Meleason, E. T.; and Johnson, D. F.: Performance Characteristics from Mach 2.58 to 1.98 of an Axisymmetric, Mixed-Compression Inlet System With 60-Percent Internal Contraction. NASA TM X 1739, 1969.

8. Sanders, Bobby W.; and Cubbison, Robert W.: Effect of Bleed-System Back Pressure and Porous Area on the Performance of an Axisymmetric Mixed-Compression Inlet at Mach 2.50. NASA TM X-1710, 1968.

9. Coltrin, Robert E.; and Choby, David A.: Steady-State Interactions from Mach 1.98 to 2.58 Between a Turbojet Engine and an Axisymmetric Inlet with 60-Percent Internal Area Contraction Systems. NASA TN X-1780, 1969.

10. Zeller, John R.: Design and Analysis of a Modular Servoamplifier for Fast-Response Electrohydraulic Control Systems. NASA TN D-4898, 1968.

11. Bowditch, David N.; and Wilcox, Fred A.: Dynamic Response of a Supersonic Diffuser to Bypass and Spike Oscillation. NASA TM X-10, 1959.

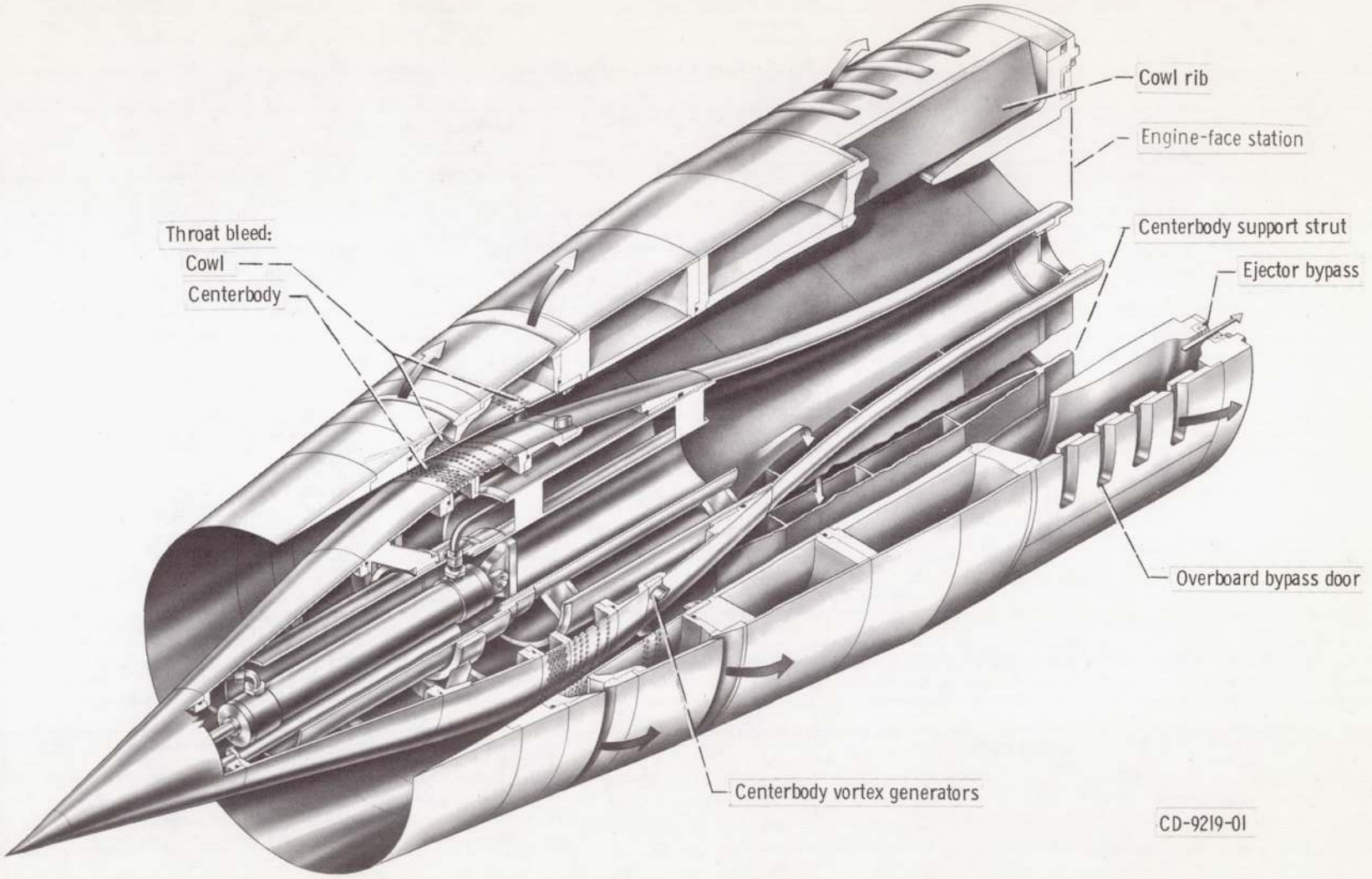

Figure 1. - Inlet model.

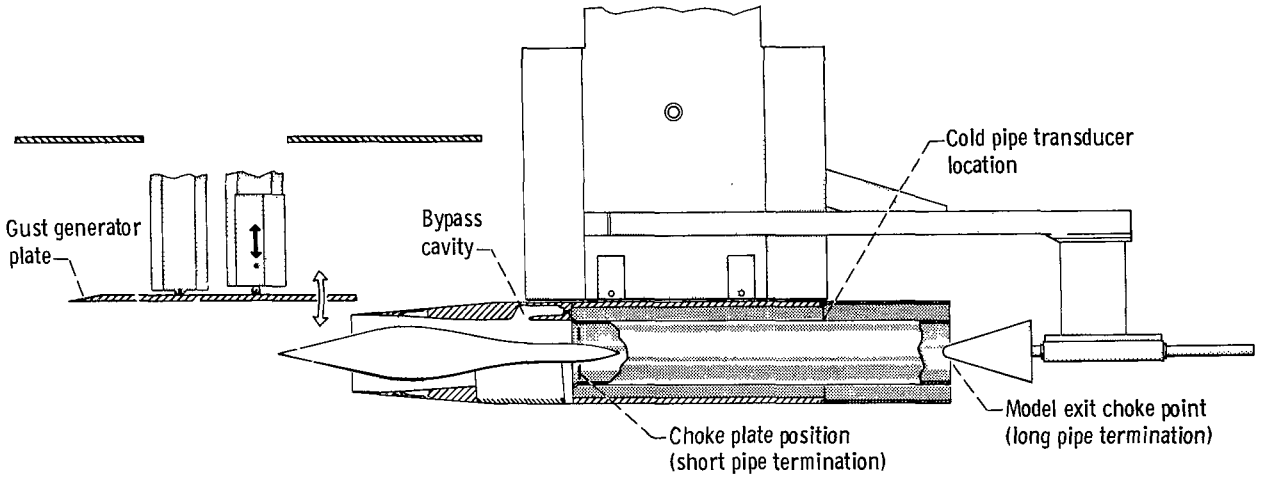

(a) Inlet cold-pipe configuration.

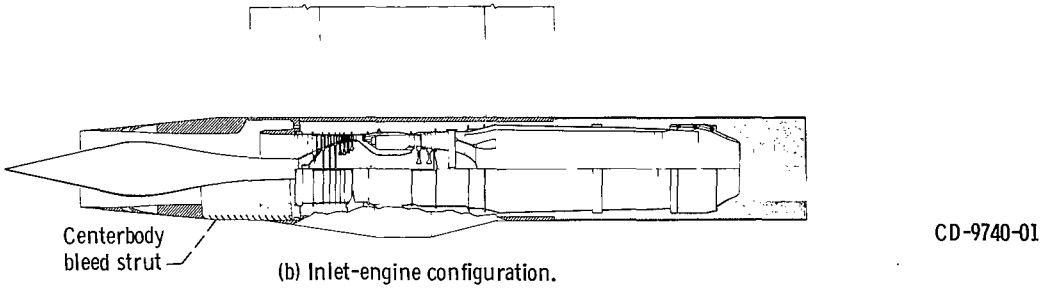

(b) Inlet-engine configuration.

Figure 2. - Test configurations.

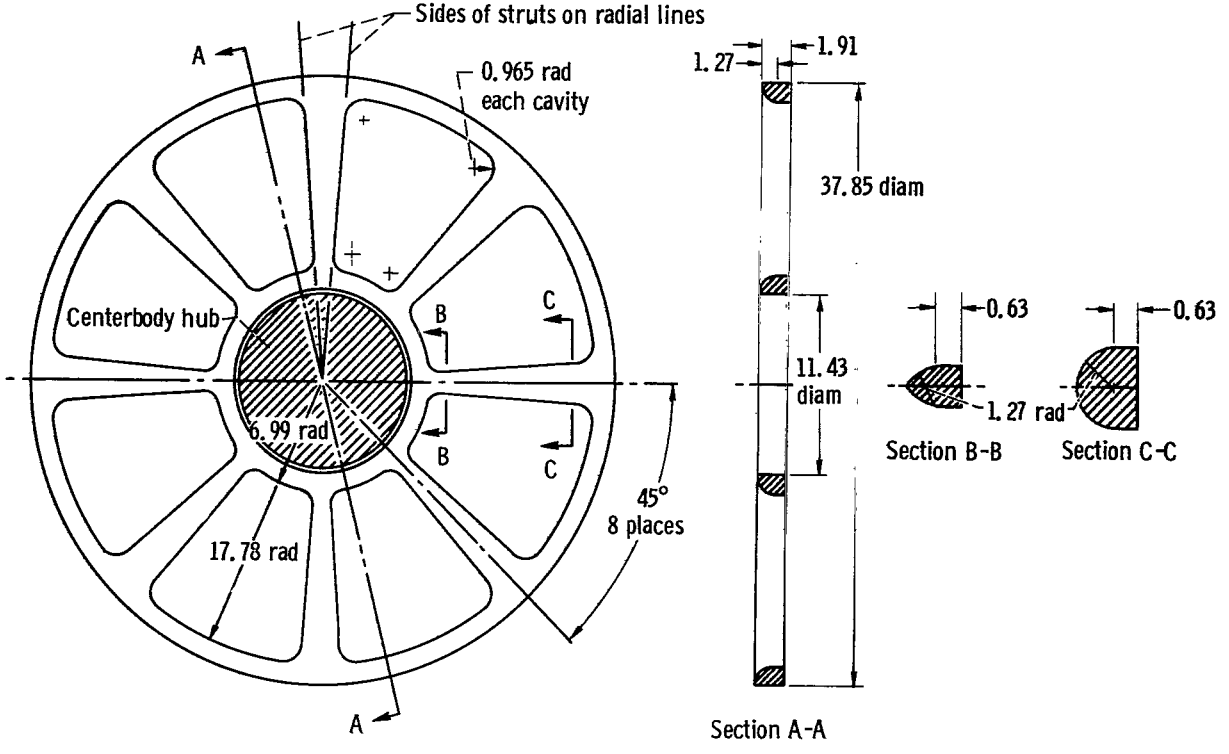

Figure 3. - Details of choke plate. Total area, 653.07 square centimeters. (All dimensions are in centimeters.)

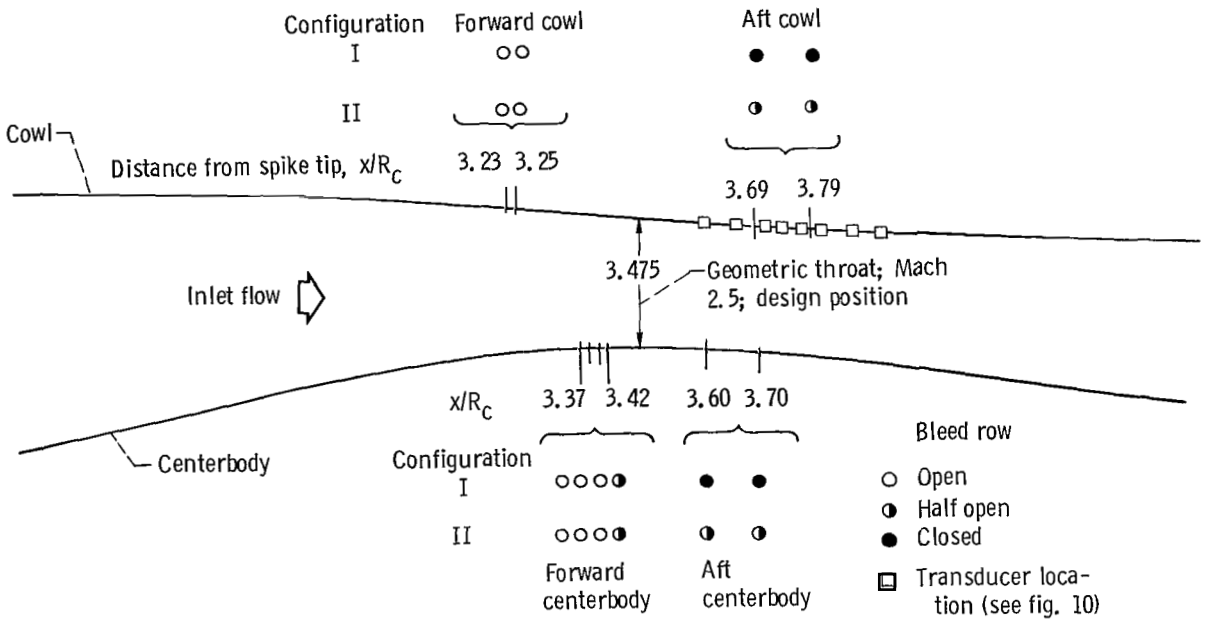

Figure 4. - Inlet bleed configurations. Bleed hole diameter, 0.3145 centimeter.

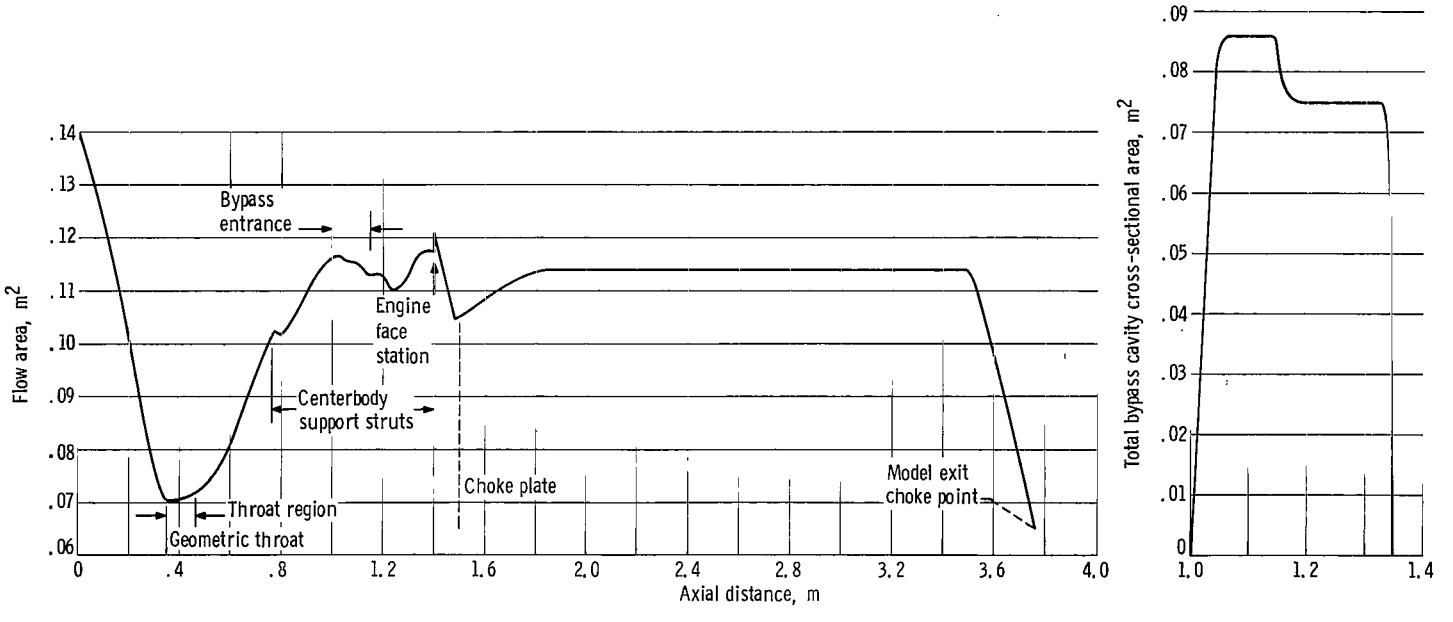

(a) Duct area.

(b) Bypass cavity cross-sectional area variation.

Figure 5. - Inlet internal area variation with distance from cowl lip.

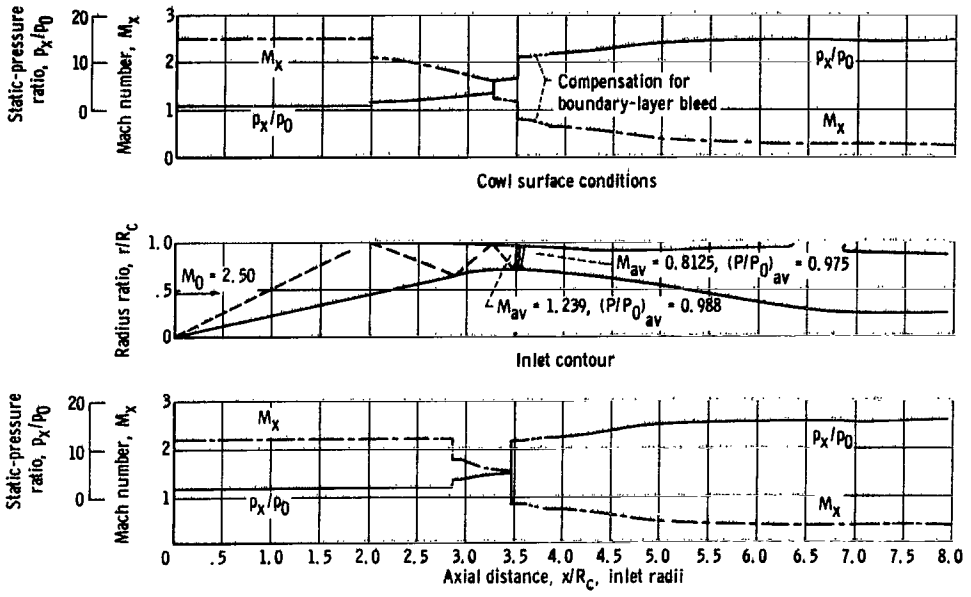

(a) Inlet dimensions and theoretical flow conditions.

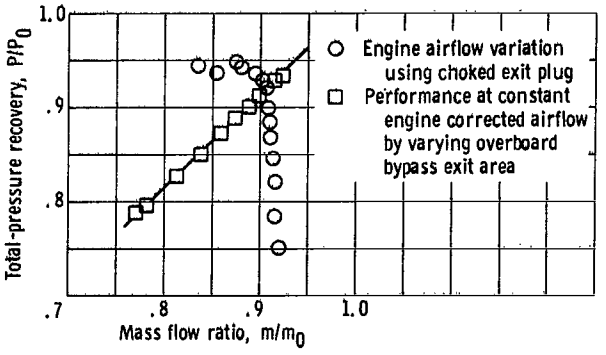

(b) Experimental performance of inlet configuration II. Engine corrected airflow, 15.83 kilograms per second.

Figure 6. - Aerodynamic details.

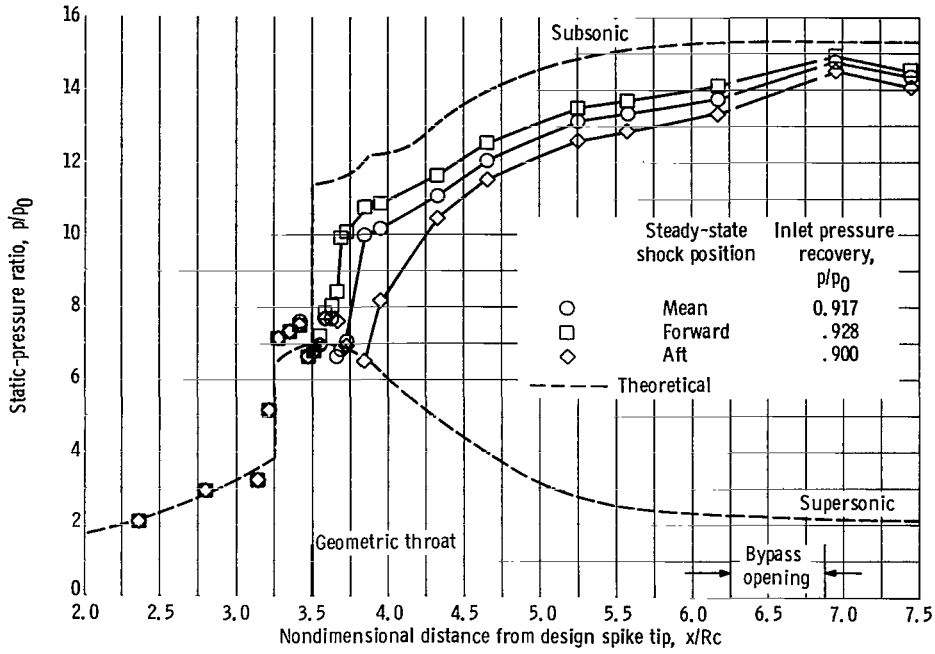

(c) Diffuser pressure distribution with the shock at mean and endpoint positions.

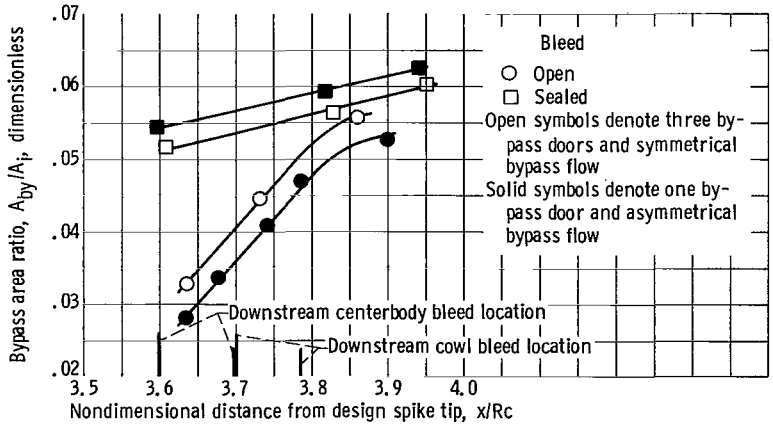

(d) Effect of bleed on shock travel in response to bypass-exit area variation. Inlet-engine configuration.

Figure 6. - Concluded.

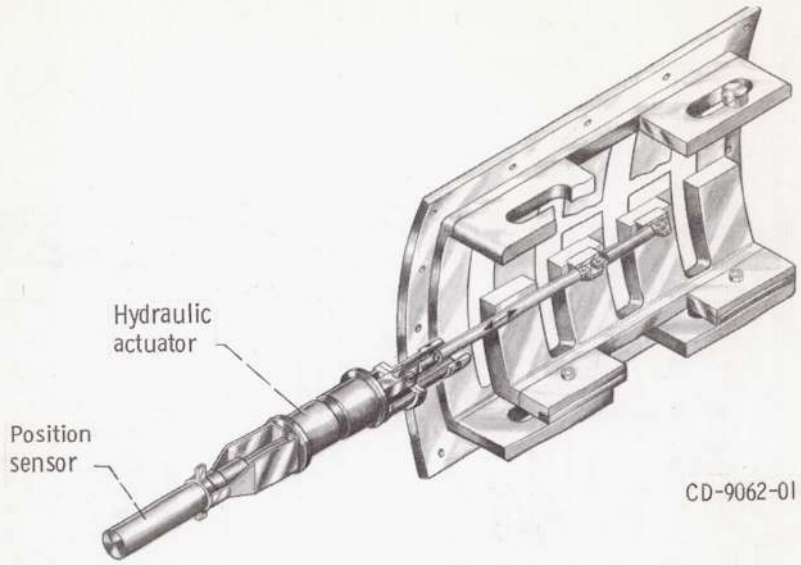

(a) Overboard bypass door assembly and actuator.

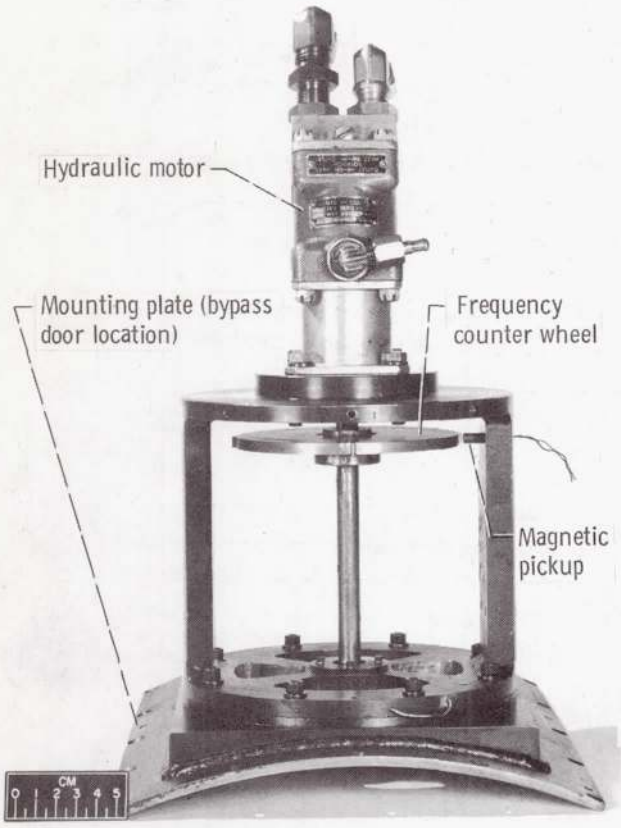

(b) Rotary valve assembly.

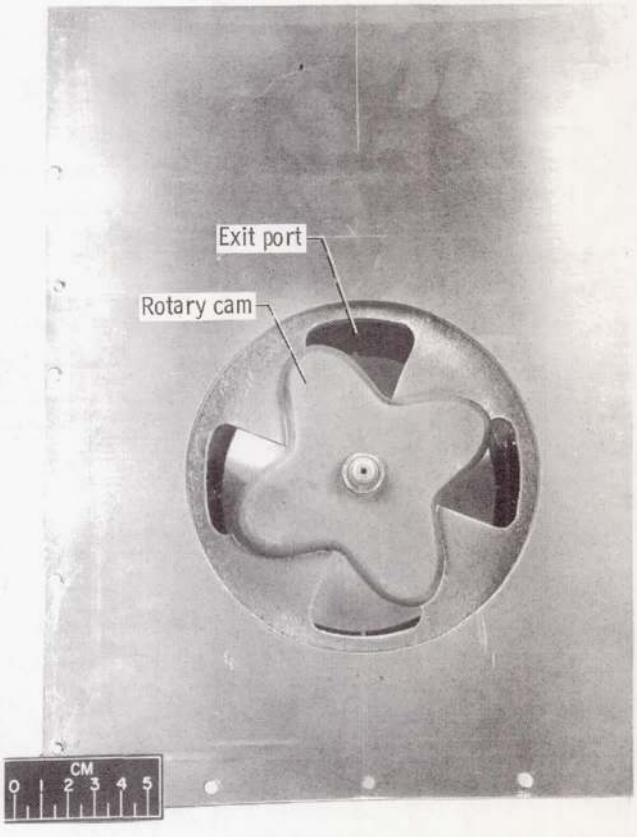

(c) Rotary valve exit details.

Figure 7. - Disturbance devices.

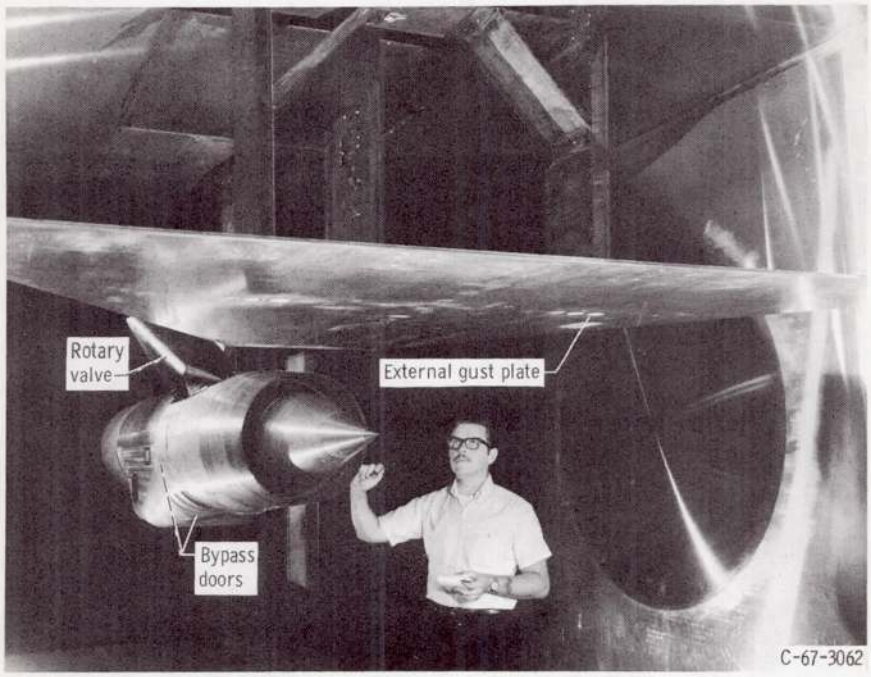

Figure 8. - Model installed in 10- by 10-Foot Supersonic Wind Tunnel.

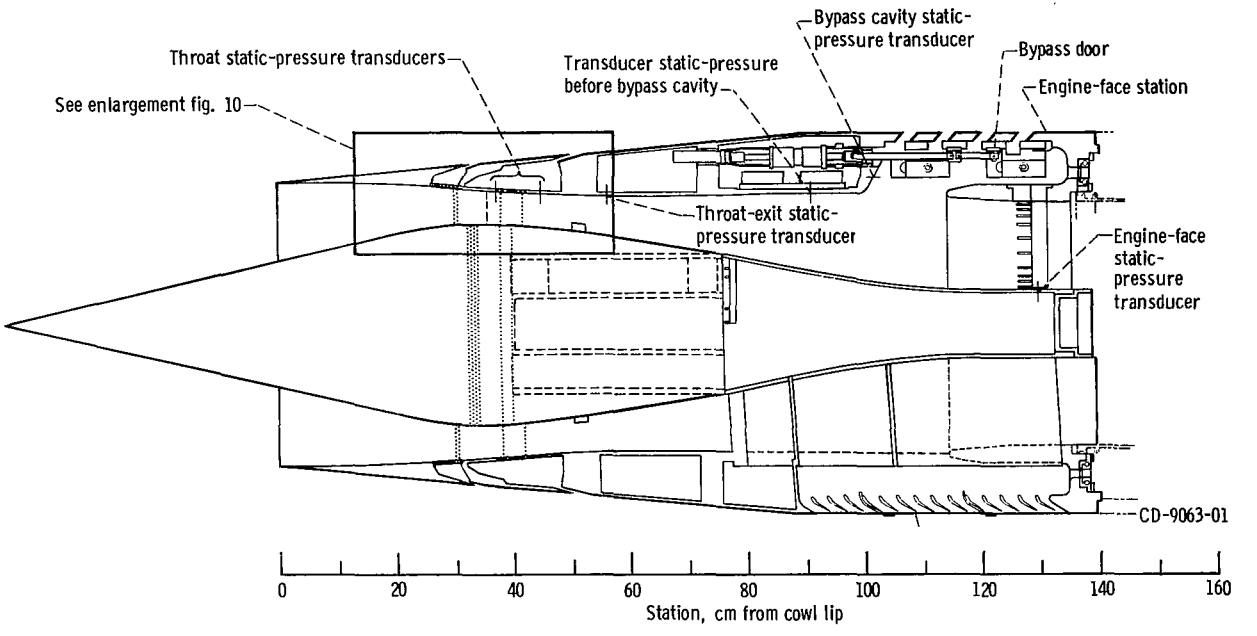

Figure 9. - Location of dynamic instrumentation.

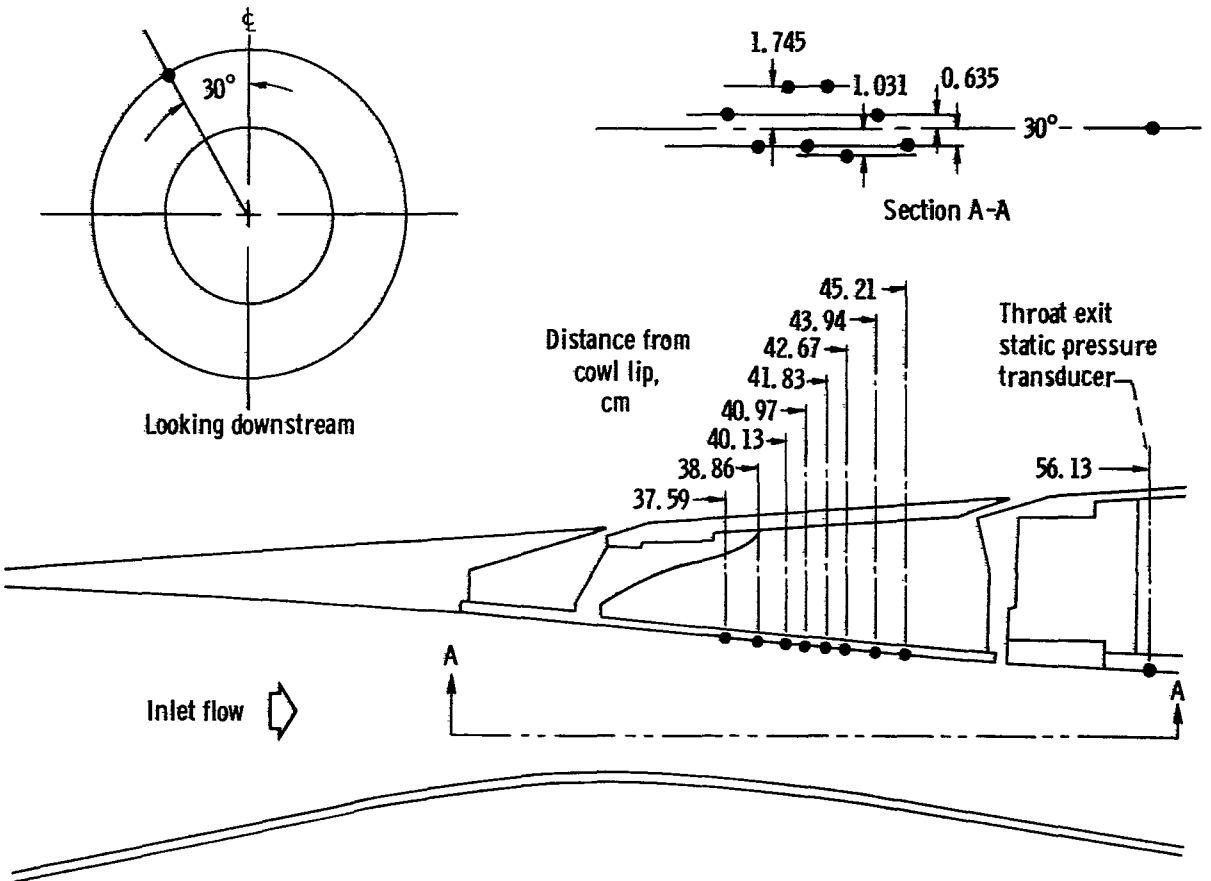

Figure 10. - Inlet throat dynamic instrumentation locations. (All dimensions are in centimeters.)

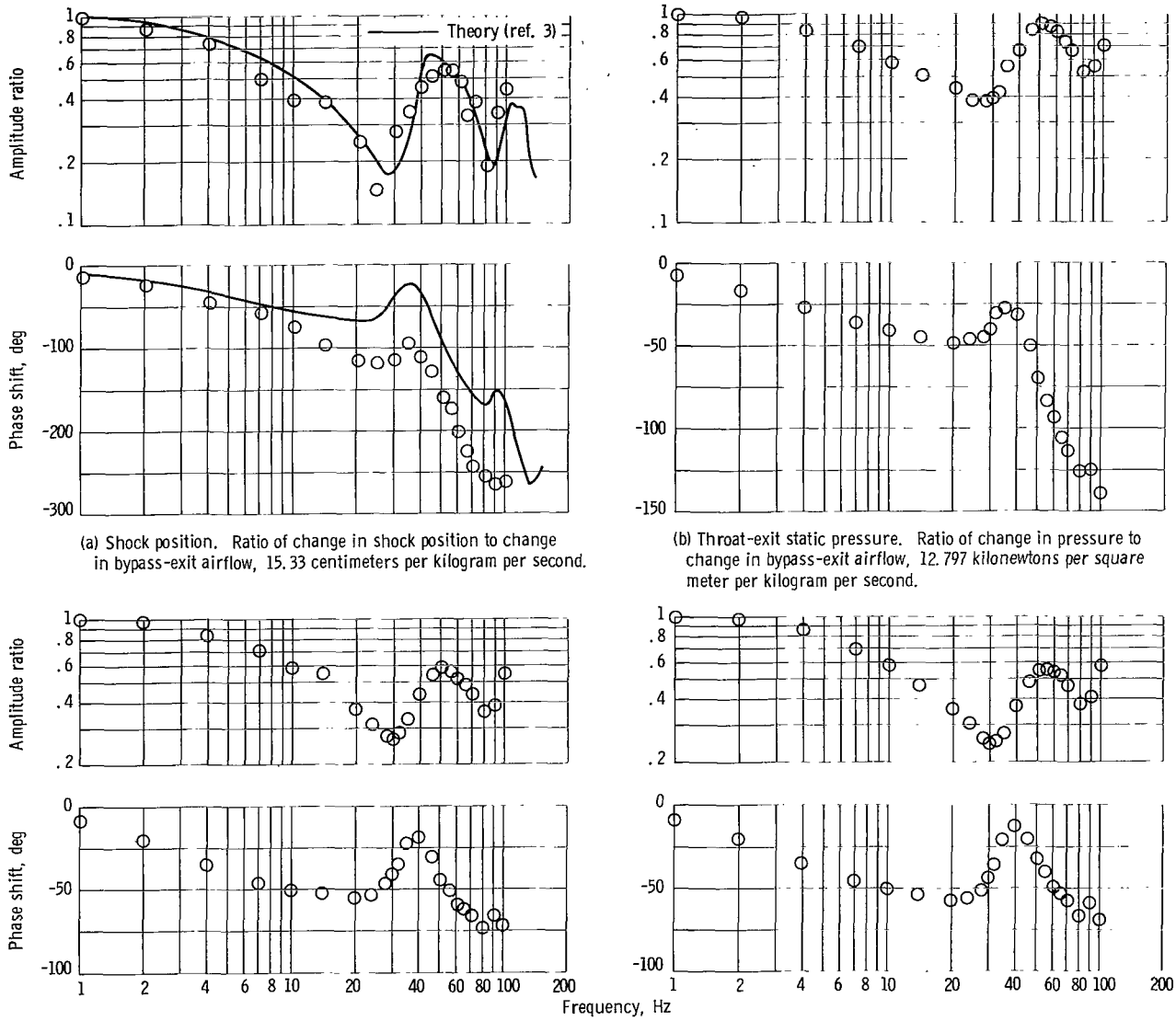

(a) Shock position. Ratio of change in shock position to change in bypass-exit airflow, 15.33 centimeters per kilogram per second.

(b) Throat-exit static pressure. Ratio of change in pressure to change in bypass-exit airflow, 12.797 kilonewtons per square meter per kilogram per second.

(c) Static pressure before bypass cavity. Ratio of change in pressure to change in bypass-exit airflow, 8.426 kilonewtons per square meter per kilogram per second.

(d) Bypass-cavity static pressure. Ratio of change in pressure to change in bypass-exit airflow, 9.264 kilonewtons per square meter per kilogram per second.

Figure 11. - Dynamic response of inlet to symmetrical internal disturbance. Long cold pipe; configuration II. Free-stream conditions: Mach number, 2.497; total pressure, 89.29 kilonewtons per meter square; total temperature, 318 K; ratio of specific heats, 1.40. Diffuser pressure recovery, 0.921; bypass airflow, 0.579 kilograms per second.

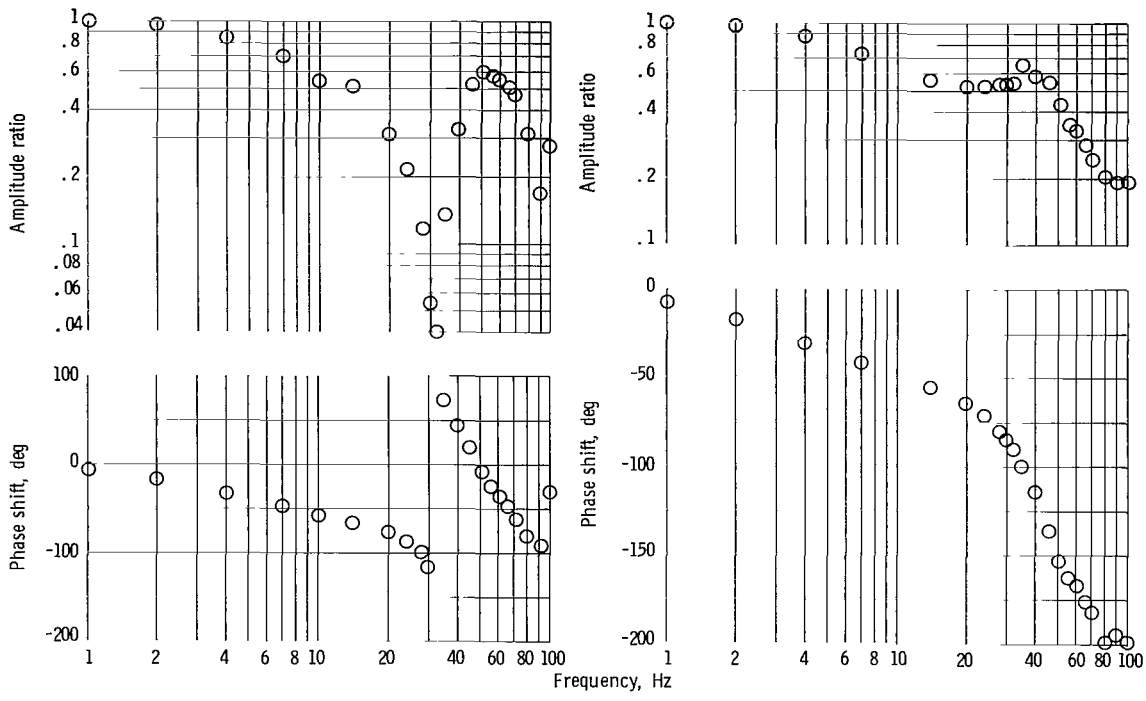

(e) Engine-face static pressure. Ratio of change in pressure to change in bypass-exit airflow, 5.119 kilonewtons per square meter per kilogram per second.

(f) Cold-flow pipe static pressure. Ratio of change in pressure to change in bypass-exit airflow, 4.977 kilonewtons per square meter per kilogram per second.

Figure 11. - Concluded.

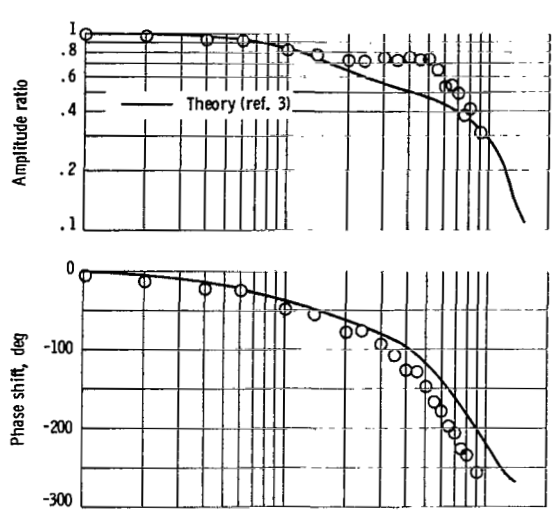

(a) Shock position. Ratio of change in shock position to change in bypass-exit airflow, 15.1 centimeters per kilogram per second.

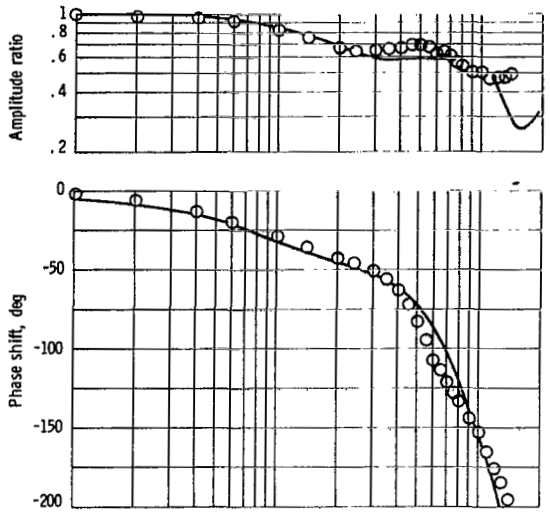

(b) Throat-exit static pressure. Ratio of change in pressure to change in bypass-exit airflow, 15.477 kilonewtons per square meter per kilogram per second.

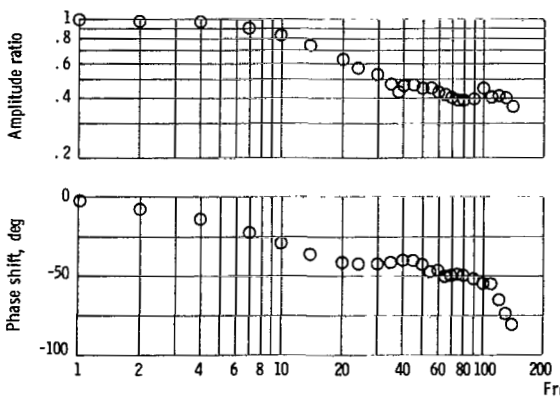

(c) Static pressure before bypass cavity. Ratio of change in pressure to change in bypass-exit airflow, 10.601 kilonewtons per square meter per kilogram per second.

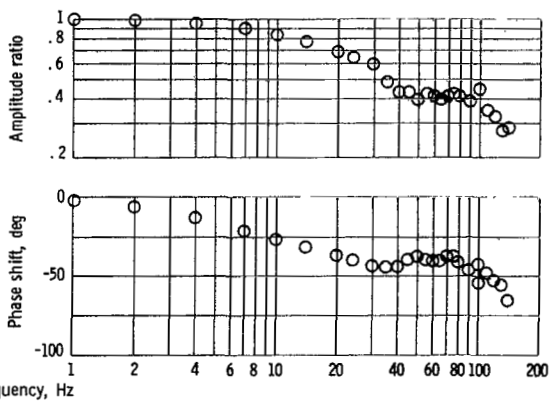

(d) Bypass-cavity static pressure. Ratio of change in pressure to change in bypass-exit airflow, 8.545 kilonewtons per square meter per kilogram per second.

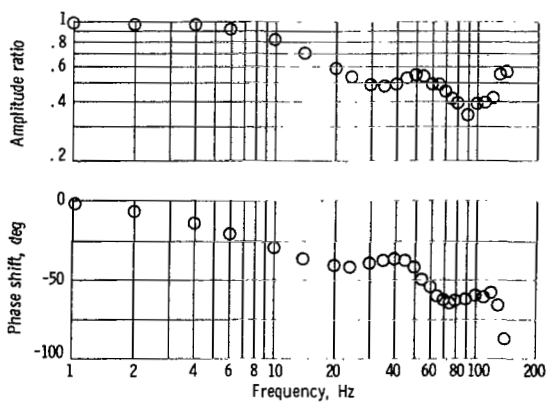

(e) Engine-face static pressure. Ratio of change in pressure to change in bypass-exit airflow, 5.112 kilonewtons per square meter per kilogram per second.

Figure 12. - Dynamic response of inlet to symmetrical internal disturbance. Choke plate; configuration II. Free-stream conditions: Mach number, 2.497; total pressure, 90.06 kilonewtons per square meter; total temperature, 316 K; ratio of specific heats, 1.400. Diffuser pressure recovery, 0.911; bypass-exit airflow disturbance amplitude, 0.609 kilogram per second.

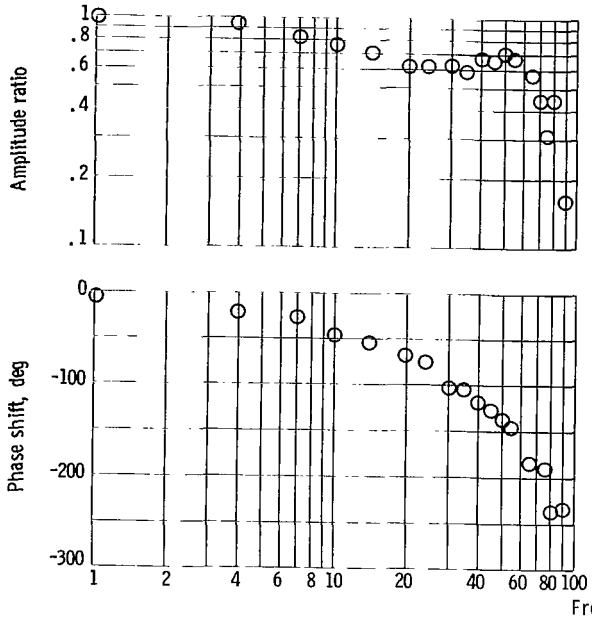

(a) Shock position. Ratio of change in shock position to change in bypass-exit airflow, 19.3 centimeters per kilogram per second.

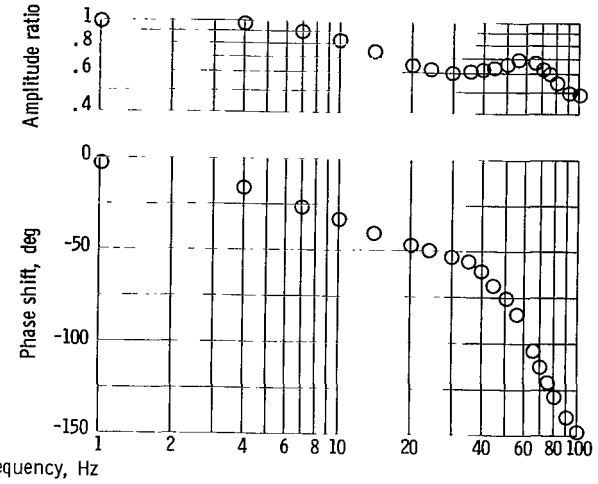

(b) Throat-exit static pressure. Ratio of change in pressure to change in bypass-exit airflow, 26.689 kilonewtons per square meter per kilogram per second.

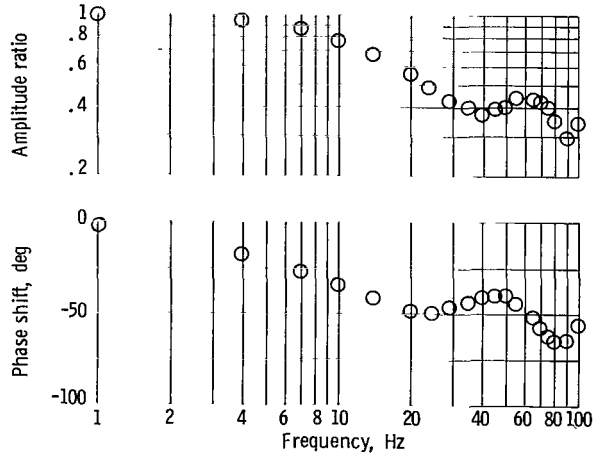

(c) Engine-face static pressure. Ratio of change in pressure to change in bypass-exit airflow, 9.229 kilonewtons per square meter per kilogram per second.

Figure 13. - Dynamic response of inlet to symmetrical internal disturbance with increased tunnel total temperature. Choke plate; configuration II. Free-stream conditions: Mach number, 2.465; total pressure, 103.78 kilonewtons per square meter; total temperature, 388 K; ratio of specific heats, 1.394. Diffuser pressure recovery, 0.928; bypass-exit airflow disturbance amplitude, 0.494 kilogram per second.

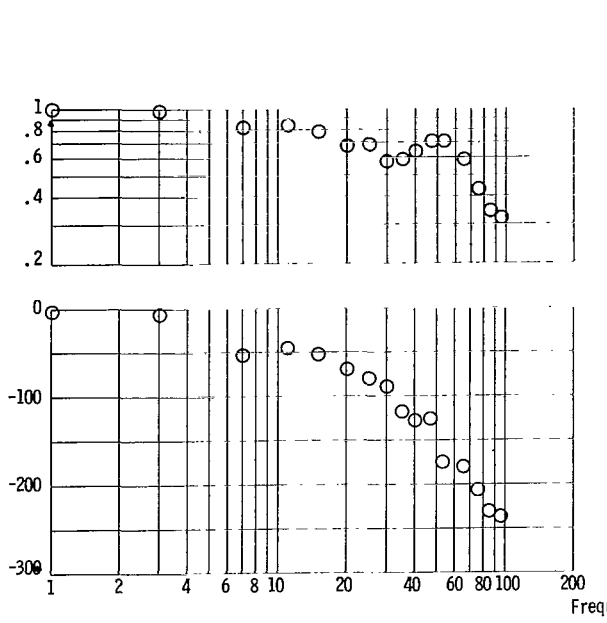

(a) Shock position. Ratio of change in shock position to change in bypass exit airflow, 11.9 centimeters per kilogram per second.

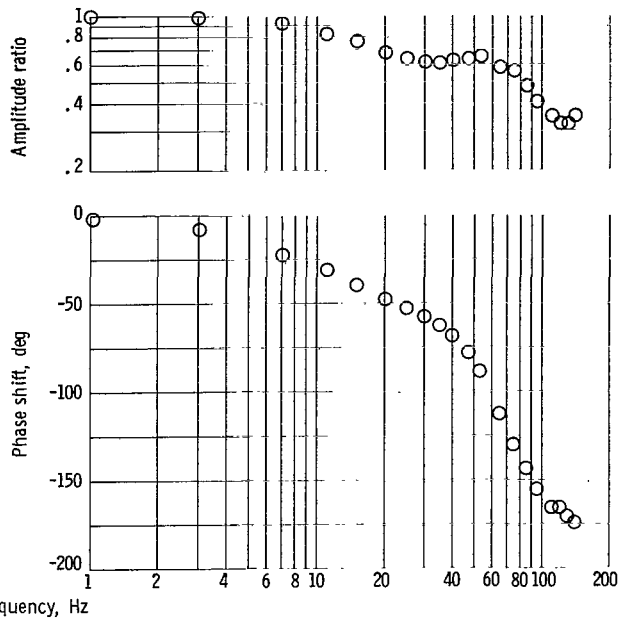

(b) Throat-exit static pressure. Ratio of change in pressure to change in bypass-exit airflow, 12.77 kilonewtons per square meter per kilogram per second.

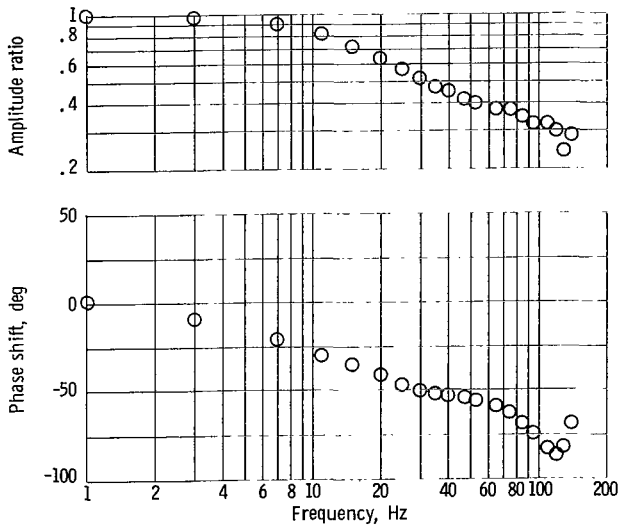

(c) Static pressure before bypass cavity. Ratio of change in pressure to change in bypass-exit airflow ratio, 8.513 kilonewtons per square meter per kilogram per second.

Figure 14. - Dynamic response of inlet to symmetrical internal disturbance. Inlet engine; configuration II. Free-stream conditions: Mach number 2.497; total pressure, 99.54 kilonewtons per square meter; total temperature, 343 K; ratio of specific heats, 1.400. Diffuser pressure recovery, 0.917; bypass-exit airflow disturbance amplitude, 0.536 kilogram per second.

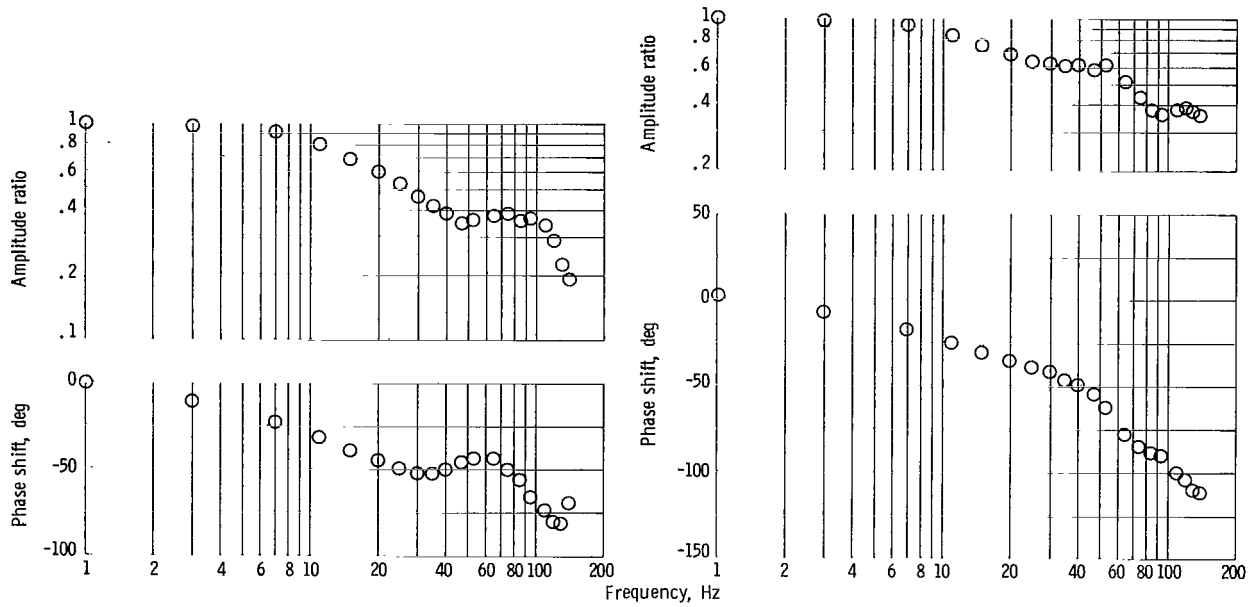

(d) Bypass-cavity static pressure. Ratio of change in pressure to change in bypass-exit airflow, 9.489 kilonewtons per square meter per kilogram per second.

(e) Engine-face static pressure. Ratio of change in pressure to change in bypass-exit airflow, 4.696 kilonewtons per square meter per kilogram per second.

Figure 14. - Concluded.

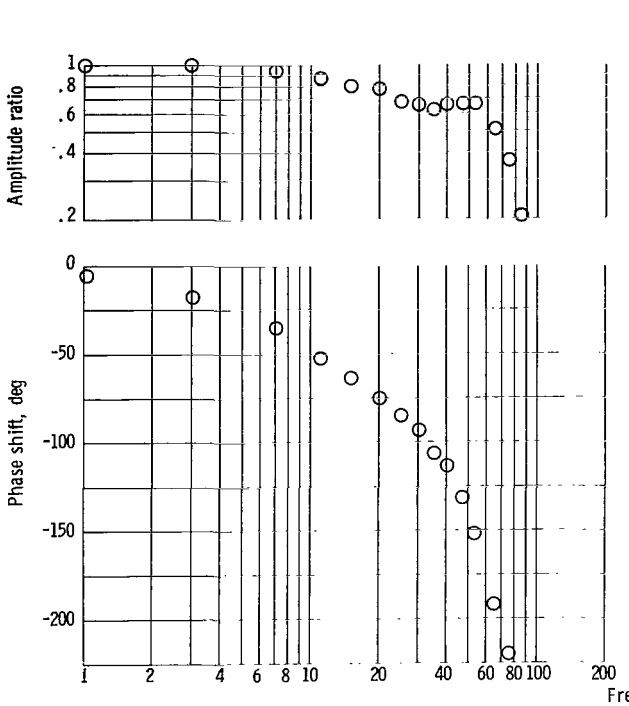

(a) Shock position. Ratio of change in shock position to change in bypass-exit airflow, 14.9 centimeters per kilogram per second.

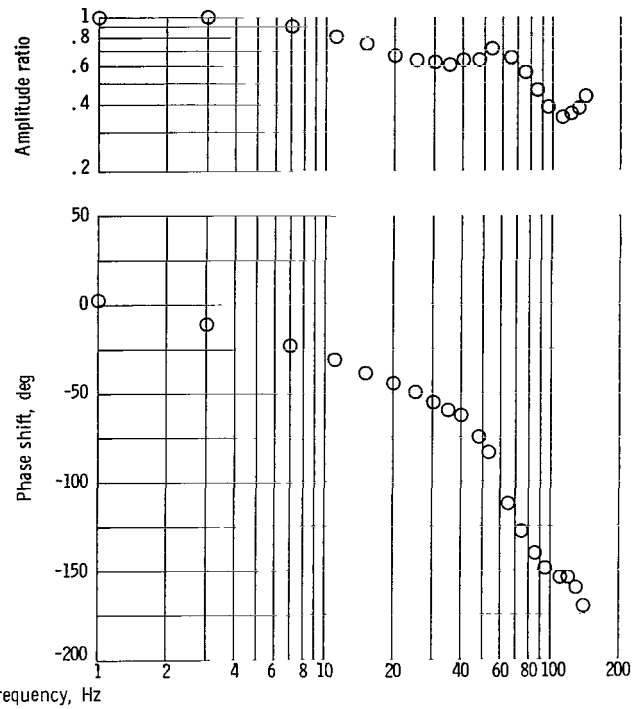

(b) Throat-exit static pressure. Ratio of change in pressure to change in bypass-exit airflow, 15.136 kilonewtons per square meter per kilogram per second.

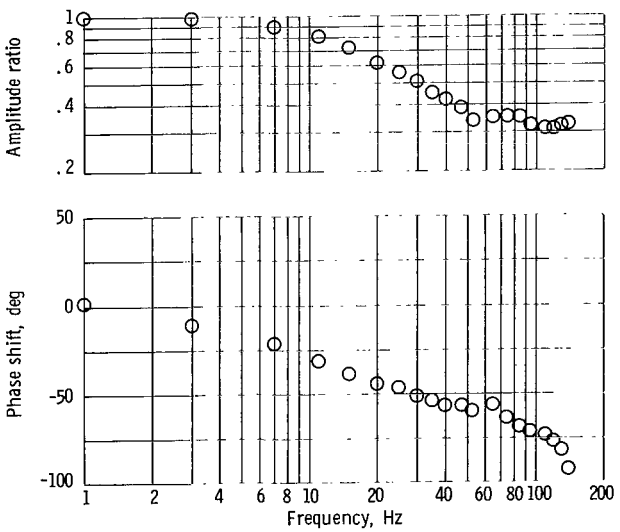

(c) Static pressure before bypass cavity. Ratio of change in pressure to change in bypass-exit airflow, 10.502 kilonewtons per square meter per kilogram per second.

Figure 15. - Dynamic response of inlet to symmetrical internal disturbance with tunnel total temperature increased. Inlet engine; configuration II. Free-stream conditions: Mach number, 2.462; total pressure, 103.20 kilonewtons per square meter; total temperature, 389 K; ratio of specific heats, 1.394. Diffuser pressure recovery, 0.927; bypass-exit airflow disturbance amplitude, 0.509 kilogram per second.

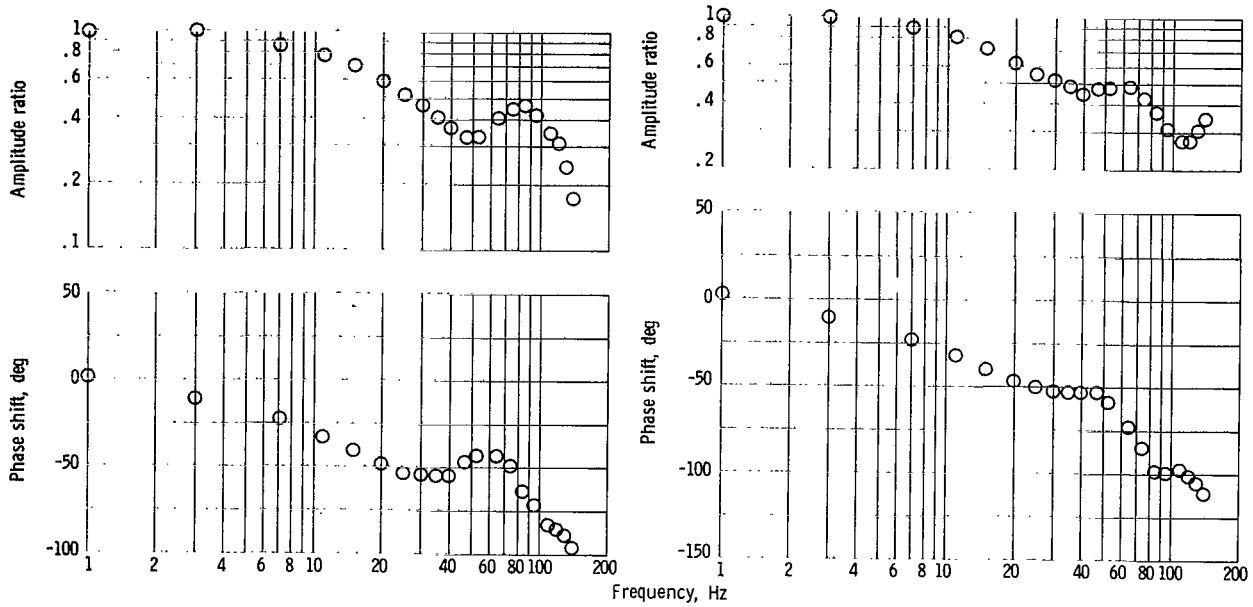

(d) Bypass-cavity static pressure. Ratio of change in pressure to change in bypass-exit airflow, 11.380 kilonewtons per square meter per kilogram per second.

(e) Engine-face static pressure. Ratio of change in pressure to change in bypass-exit airflow, 6.569 kilonewtons per square meter per kilogram per second.

Figure 15. - Concluded.

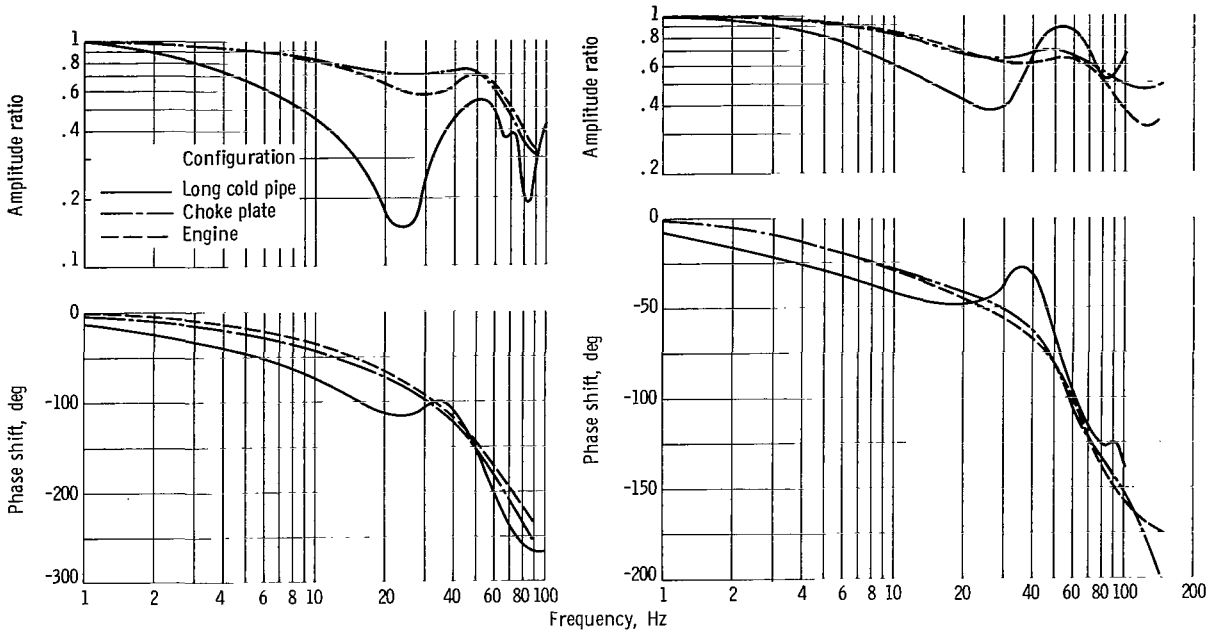

(a) Shock position.

(b) Throat-exit static pressure.

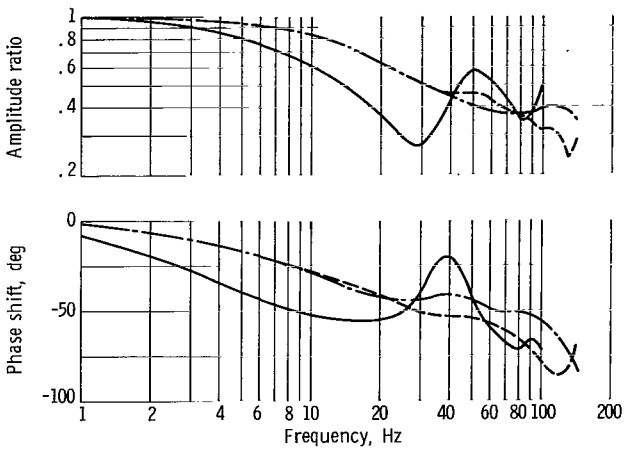

(c) Static pressure before bypass cavity.

Figure 16. - Comparison of inlet dynamic response obtained from internal symmetrical disturbance for three inlet terminations; configuration II.

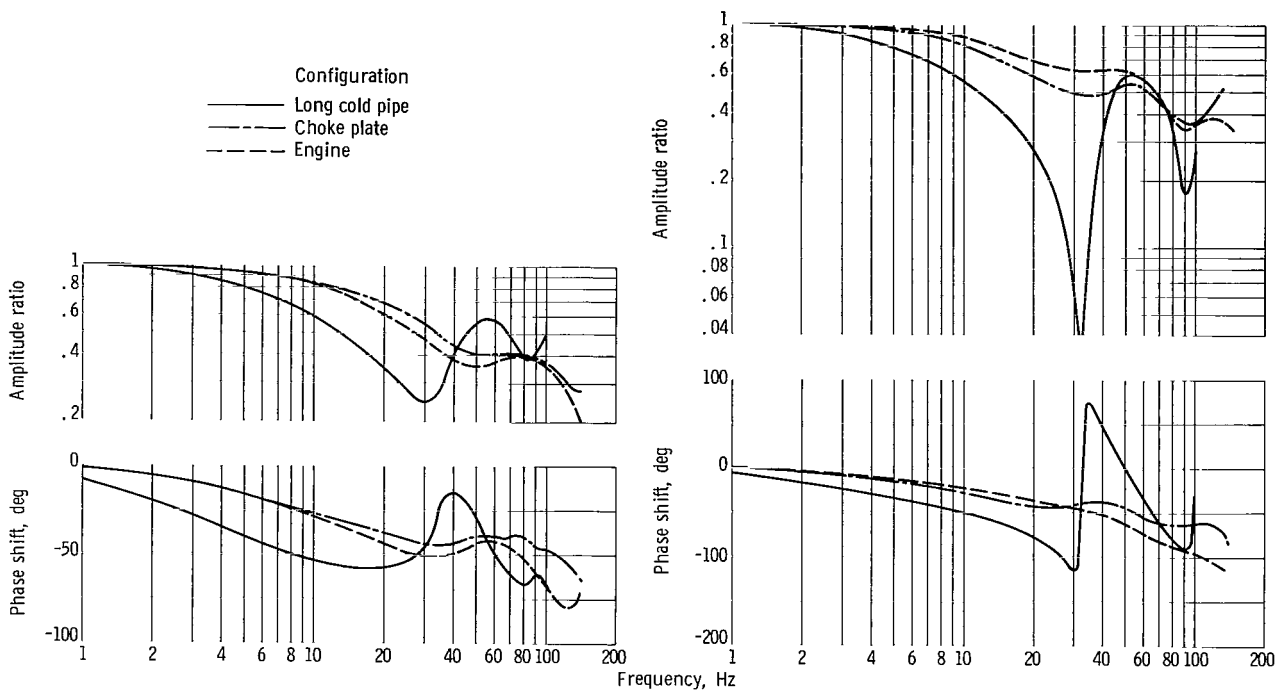

(d) Bypass-cavity static pressure.

(e) Engine-face static pressure.

Figure 16. - Concluded.

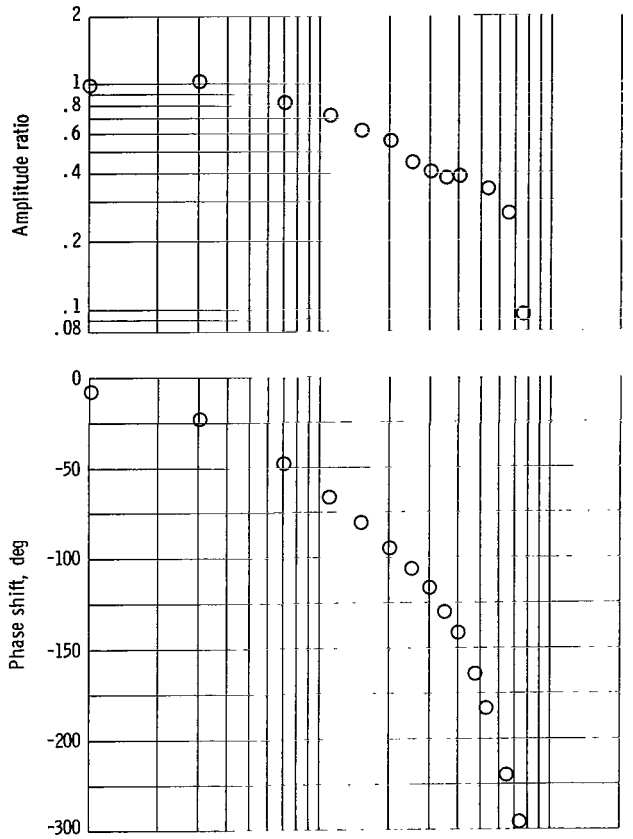

(a) Shock position. Ratio of change in shock position to change in bypass-exit airflow, 51.6 centimeters per kilogram per second.

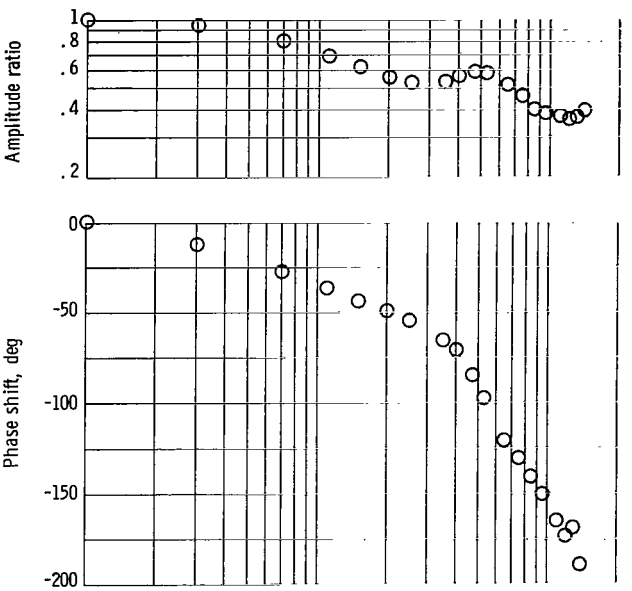

(b) Throat-exit static pressure. Ratio of change in pressure to change in bypass-exit airflow, 13.168 kilonewtons per square meter per kilogram per second.

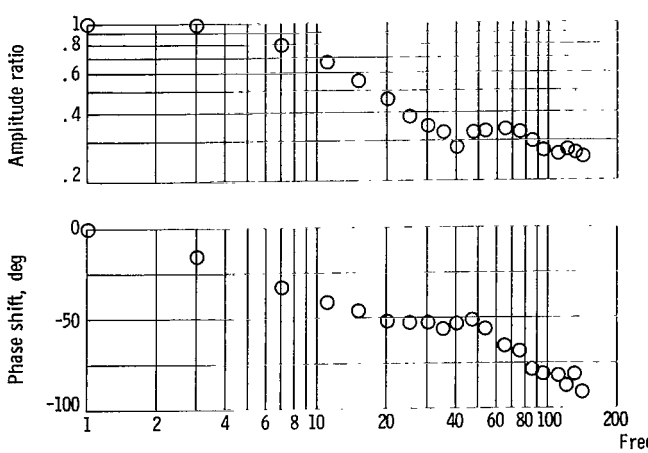

(c) Static pressure before bypass cavity. Ratio of change in pressure to change in bypass-exit airflow, 9.581 kilonewtons per square meter.

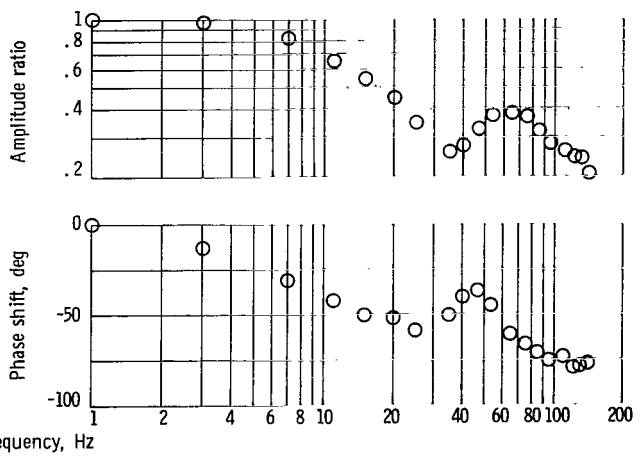

(d) Bypass-cavity static pressure. Ratio of change in pressure to change in bypass-exit airflow, 9.872 kilonewtons per square meter per kilogram per second.

Figure 17. - Dynamic response of inlet to symmetrical internal disturbance. Inlet engine; configuration I. Free-stream conditions; Mach number 2.497; total pressure, 99.13 kilonewtons per square meter: total temperature, 344 K; ratio of specific heats, 1.400. Diffuser pressure recovery, 0.910; bypass-exit airflow disturbance amplitude, 0.214 kilogram per second.

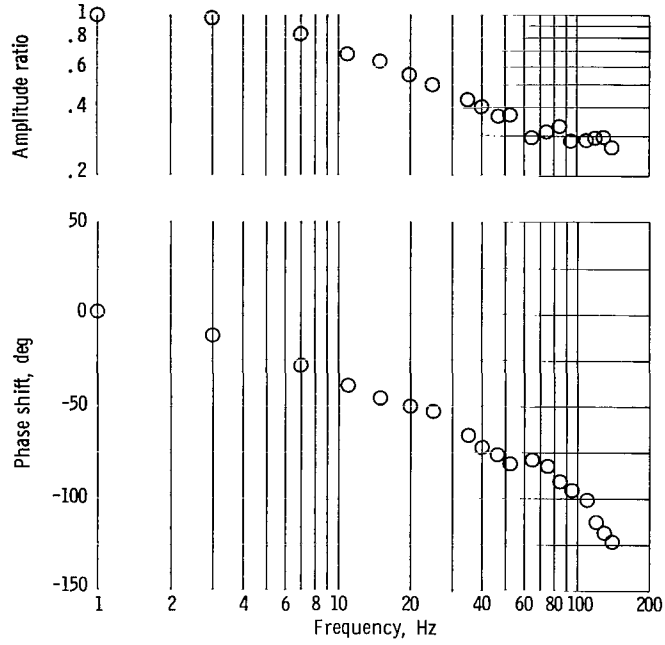

(e) Engine-face static pressure. Ratio of change in pressure to change in bypass-exit airflow, 5.809 kilonewtons per square meter per kilogram per second.

Figure 17. - Concluded.

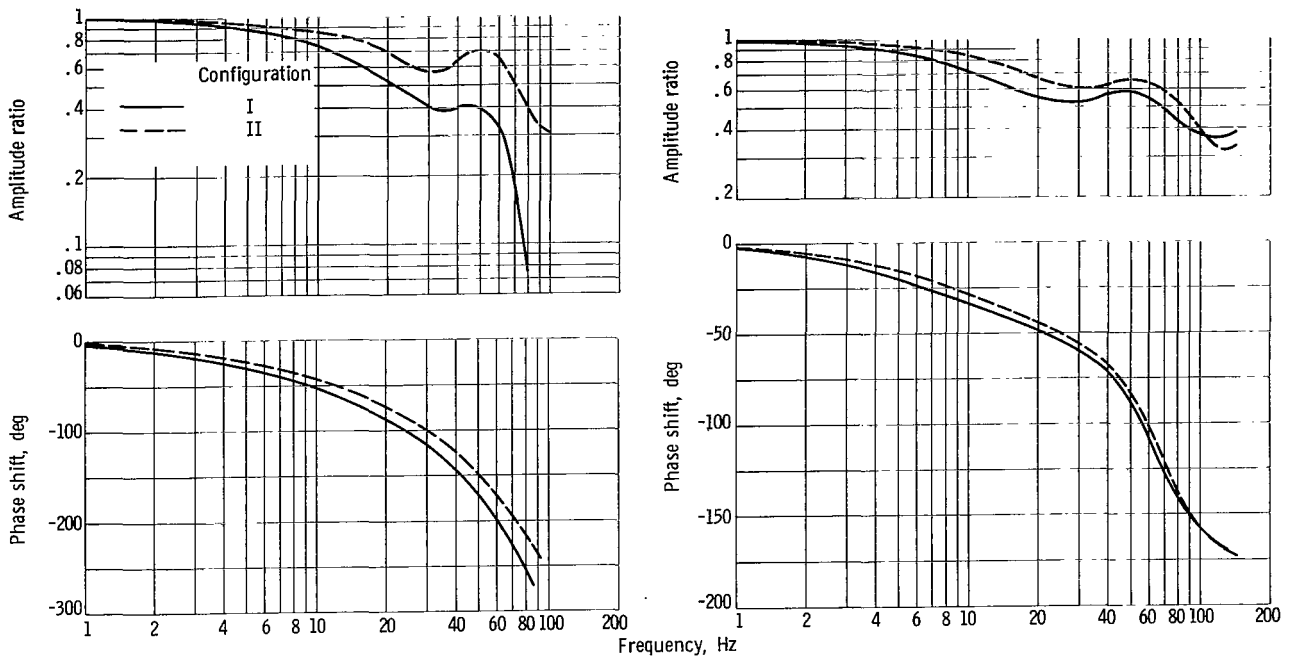

(a) Shock position.

(b) Throat-exit static pressure.

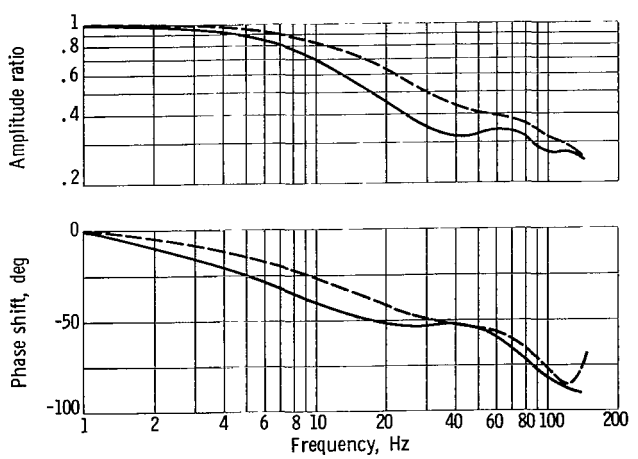

(c) Static pressure before bypass cavity.

Figure 18. - Effect of inlet throat bleed on inlet dynamic response obtained from symmetrical internal disturbance for the inlet-engine configuration.

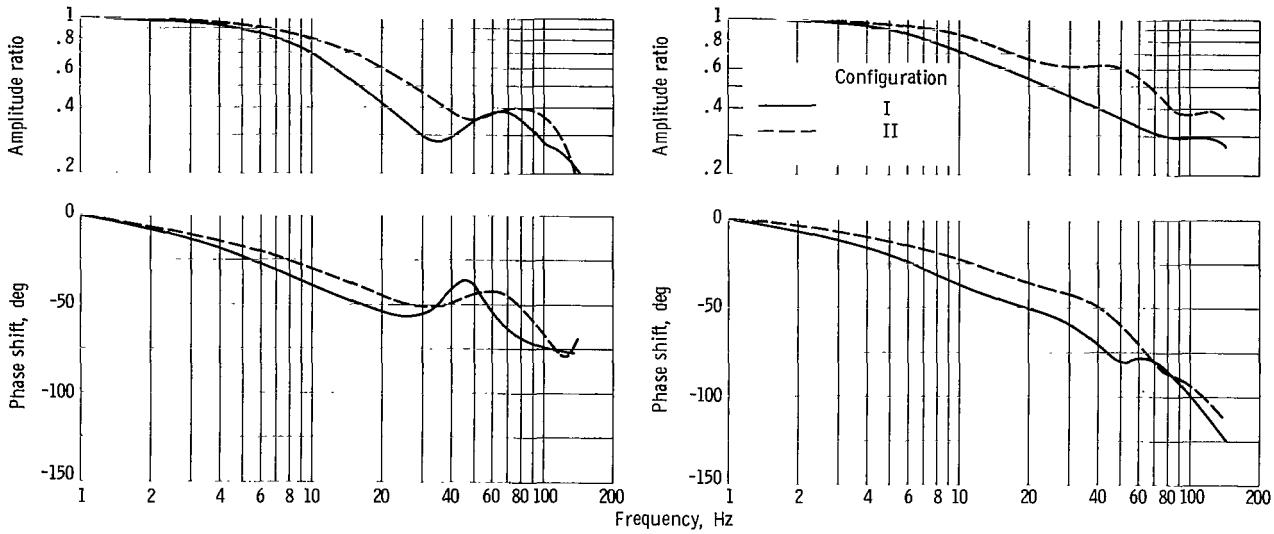

(d) Bypass-cavity static pressure.

(e) Engine-face static pressure.

Figure 18. - Concluded.

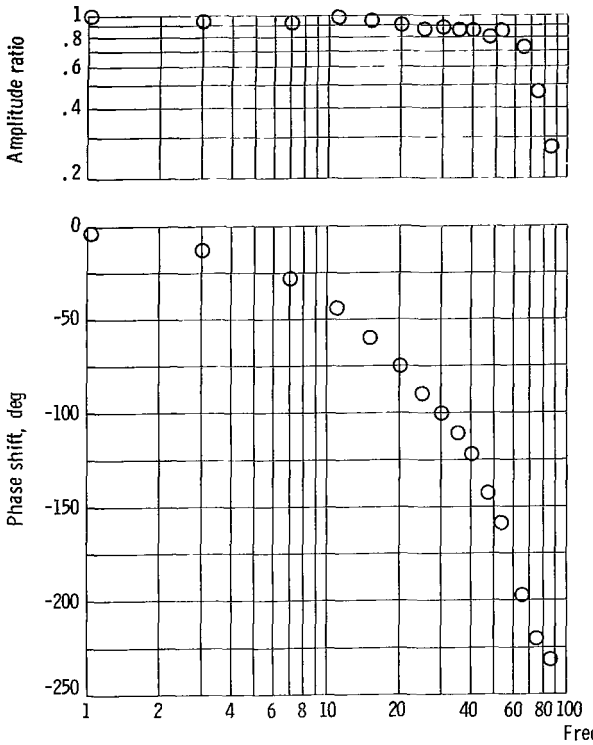

(a) Shock position. Ratio of change in shock position to change in bypass-exit airflow, 12.1 centimeters per kilogram per second.

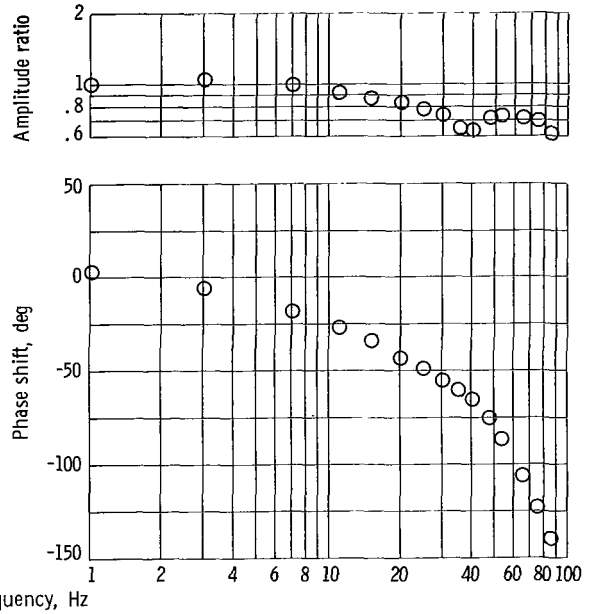

(b) Throat-exit static pressure. Ratio of change in pressure to change in bypass-exit airflow, 13.999 kilonewtons per square meter per kilogram per second.

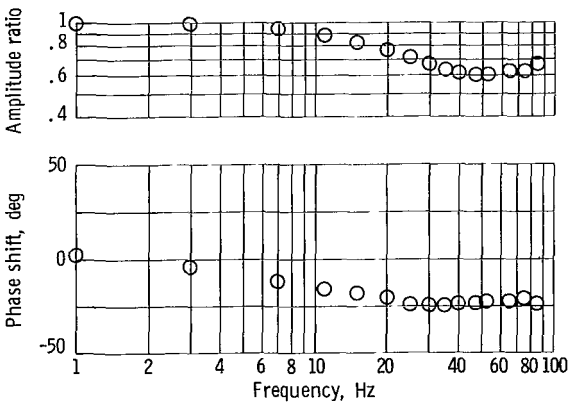

(c) Static pressure before bypass cavity. Ratio of change in pressure to change in bypass-exit airflow, 15.47 kilonewtons per square meter per kilogram per second.

Figure 19. - Dynamic response of inlet to unsymmetrical bypass door internal disturbance. Inlet engine; configuration II. Free-stream conditions: Mach number, 2.497; total pressure, 100.19 kilonewtons per square meter; total temperature, 343 K; ratio of specific heats, 1.400. Diffuser pressure recovery, 0.917; bypass-exit airflow disturbance amplitude, 0.295 kilogram per second.

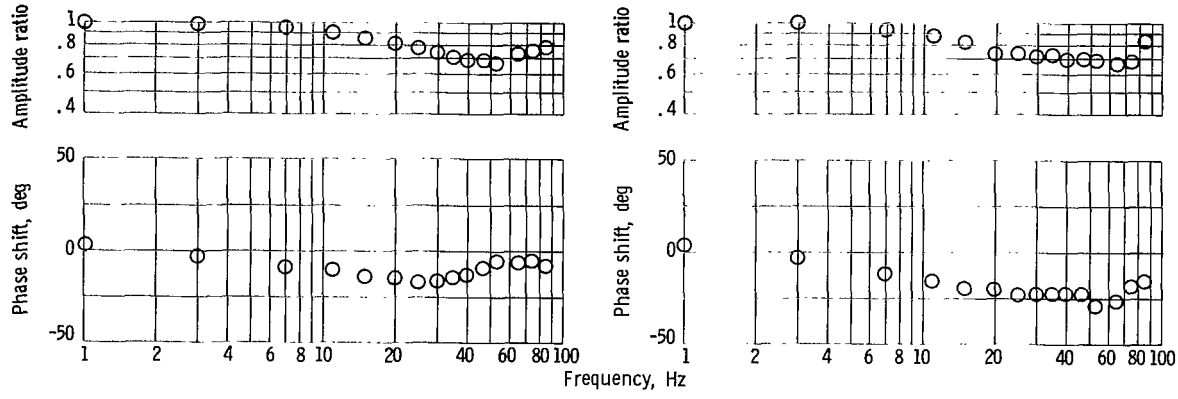

(d) Bypass-cavity static pressure. Ratio of change in pressure to change in bypass-exit airflow, 11.205 kilonewtons per square meter per kilogram per second.

(e) Engine-face static pressure. Ratio of change in pressure to change in bypass-exit airflow, 4.670 kilonewtons per square meter per kilogram per second.

Figure 19. - Concluded.

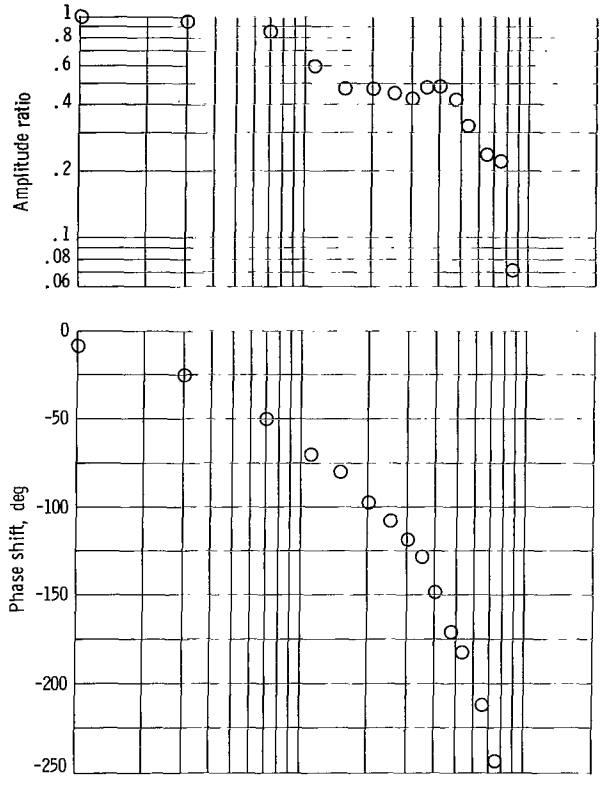

(a) Shock position. Ratio of change in shock position to change in bypass-exit airflow, 61.9 centimeters per kilogram per second.

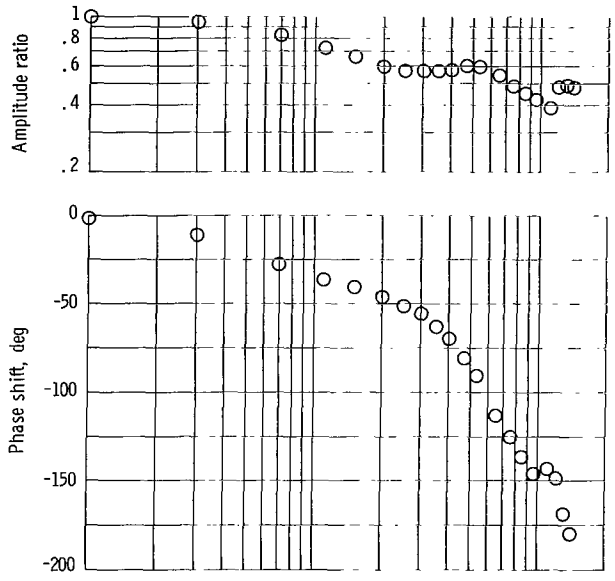

(b) Throat-exit static pressure. Ratio of change in pressure to change in bypass-exit airflow, 17.128 kilonewtons per square meter per kilogram per second.

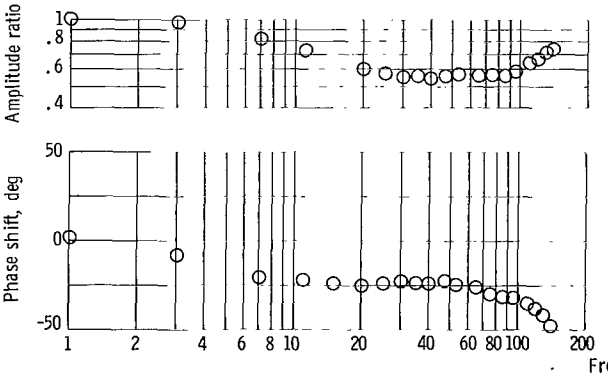

(c) Static pressure before bypass cavity. Ratio of change in pressure to change in bypass-exit airflow, 18.948 kilonewtons per square meter per kilogram per second.

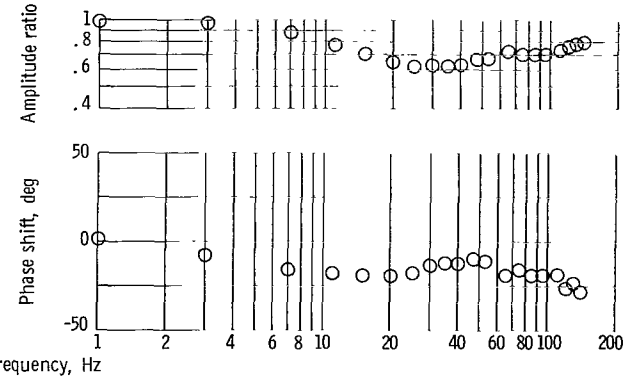

(d) Bypass-cavity static pressure. Ratio of change in pressure to change in bypass-exit airflow, 13.210 kilonewtons per square meter per kilogram per second.

Figure 20. - Dynamic response of inlet to unsymmetrical bypass-door internal disturbance. Inlet engine; configuration I. Free-stream conditions: Mach number, 2.497; total pressure, 99.47 kilonewtons per square meter; total temperature, 344 K; ratio of specific heats, 1.400. Diffuser pressure recovery, 0.915; bypass-exit airflow disturbance amplitude, 0.164 kilogram per second.

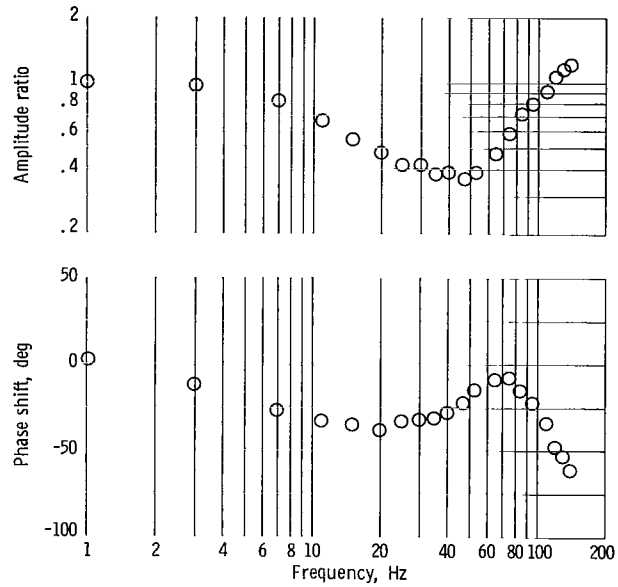

(e) Engine-face static pressure. Ratio of change in pressure to change in bypass-exit airflow, 5.998 kilonewtons per square meter per kilogram per second.

Figure 20. - Concluded.

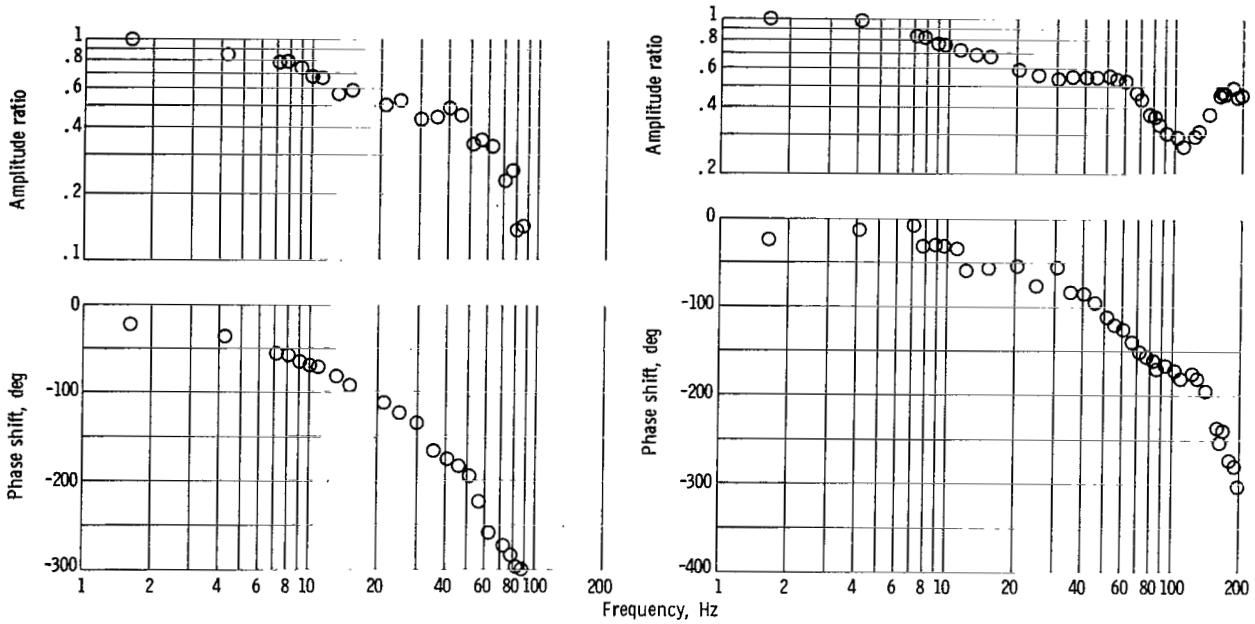

(a) Shock position. Ratio of change in shock position to change in bypass-exit airflow ratio, 54.2 centimeters per kilogram per second.

(b) Throat-exit static pressure. Ratio of change in pressure to change in bypass-exit airflow, 13.497 kilonewtons per square meter per kilogram per second.

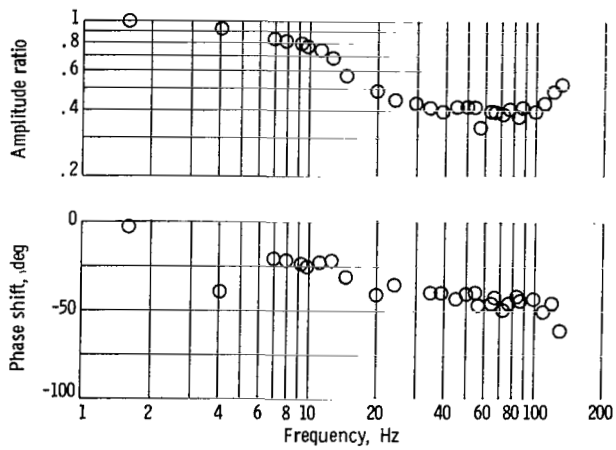

(c) Static pressure before bypass cavity. Ratio of change in pressure to change in bypass-exit airflow, 9.156 kilonewtons per square meter per kilogram per second.

Figure 21. - Dynamic response of inlet to unsymmetrical rotary valve internal disturbance. Choke plate; configuration I. Free-stream conditions: Mach number, 2.497; total pressure, 89.91 kilonewtons per square meter; total temperature, 316 K; ratio of specific heats, 1.400. Diffuser pressure recovery, 0.917; bypass-exit airflow disturbance amplitude, 0.253 kilogram per second.

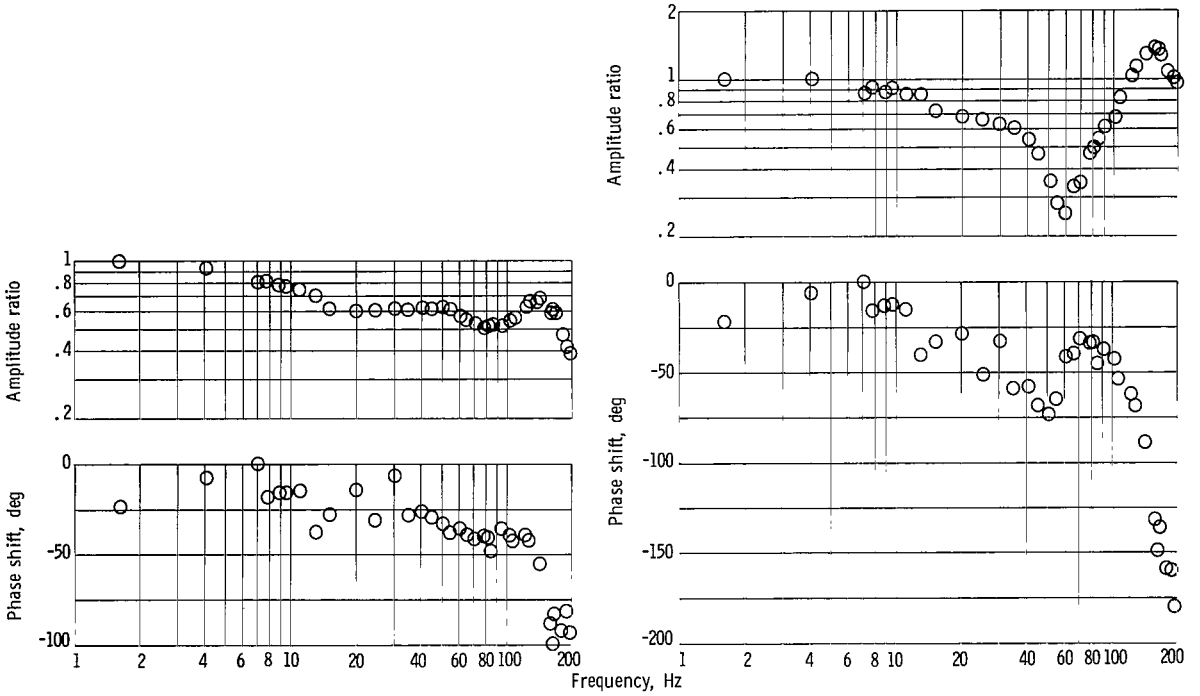

(d) Bypass-cavity static pressure. Ratio change in pressure to change in bypass-exit airflow, 9.413 kilonewtons per square meter per kilogram per second.

(e) Engine-face static pressure. Ratio of change in pressure to change in bypass-exit airflow, 4.937 kilonewtons per square meter per kilogram per second.

Figure 21. - Concluded.

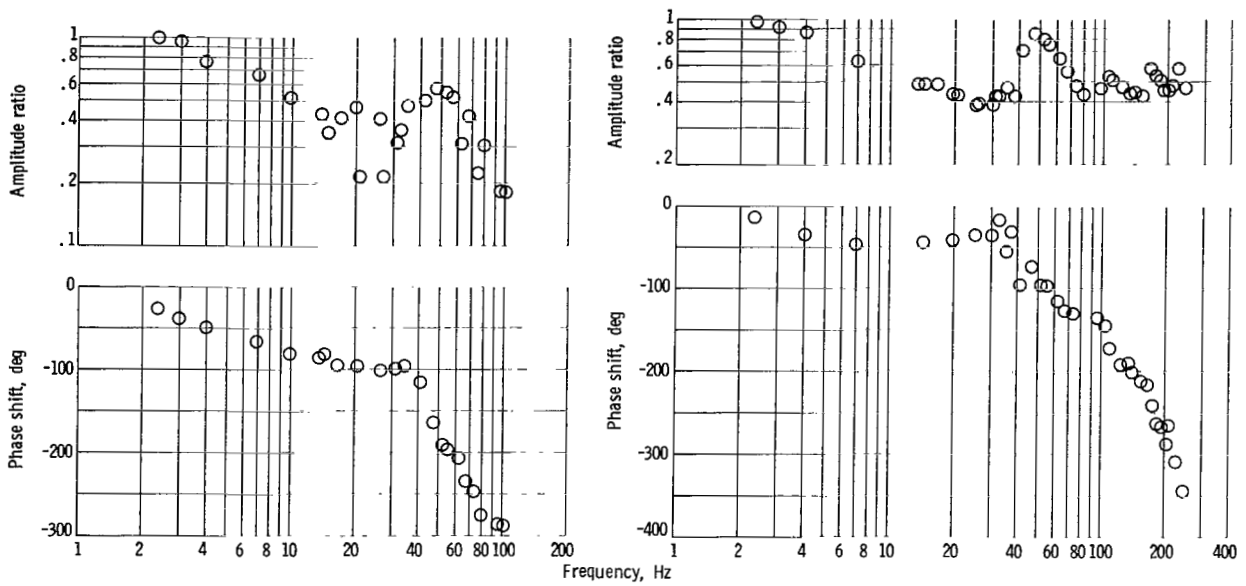

(a) Shock position. Ratio of change in shock position to change in bypass-exit airflow, 42.7 centimeters per kilogram per second.

(b) Throat-exit static pressure. Ratio of change in pressure to change in bypass-exit airflow, 13.386 kilonewtons per square meter per kilogram per second.

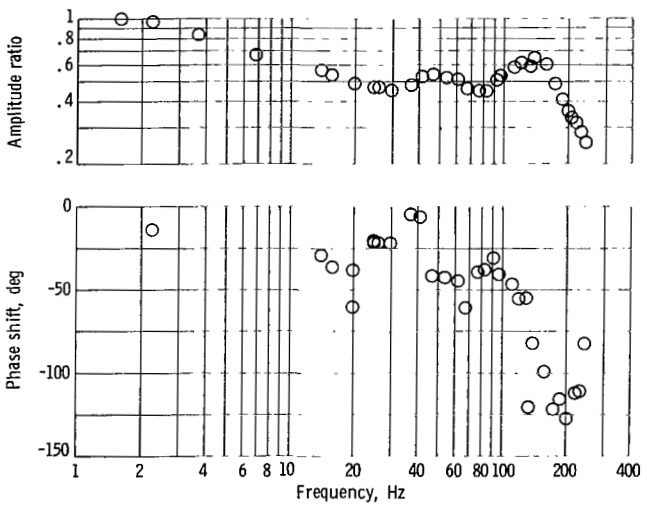

(c) Static pressure before bypass cavity. Ratio of change in pressure to change in bypass-exit airflow, 9.088 kilonewtons per square meter per kilogram per second.

Figure 22. - Dynamic response of inlet to unsymmetrical rotary valve internal disturbance. Long cold pipe; configuration I. Free-stream conditions: Mach number, 2.497; total pressure, 89.14 kilonewtons per square meter; total temperature, 318 K; ratio of specific heats, 1.400. Diffuser pressure recovery, 0.903; bypass-exit airflow disturbance amplitude, 0.253 kilogram per second.

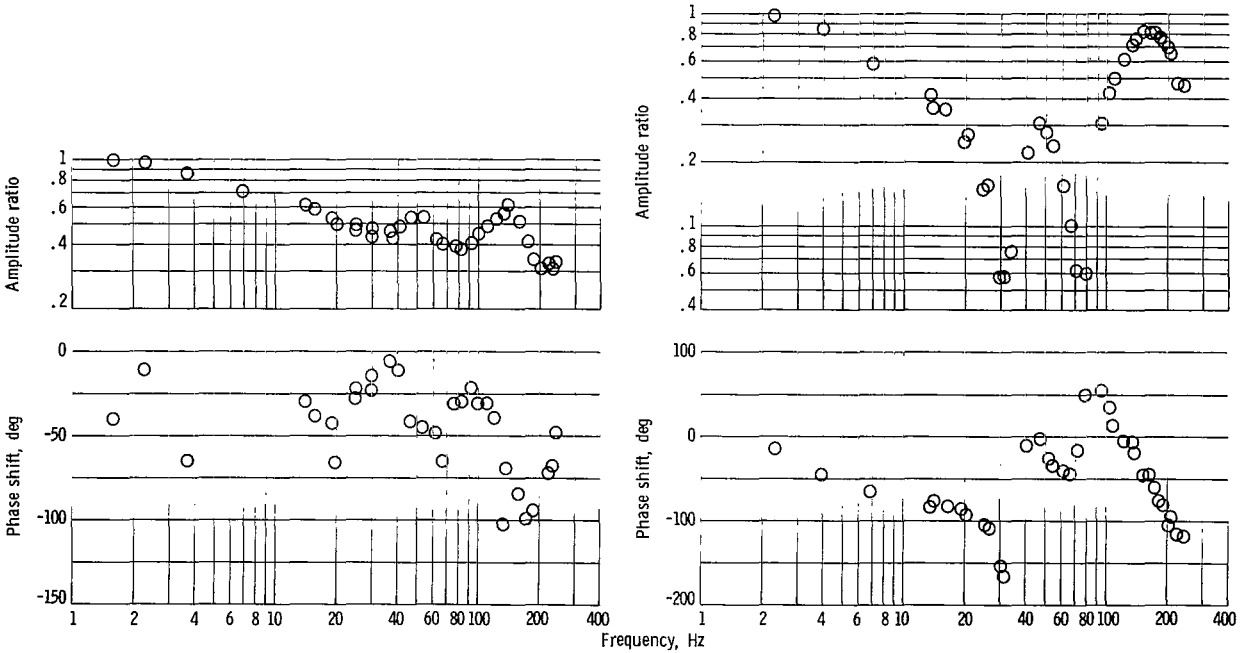

(d) Bypass-cavity static pressure. Ratio of change in pressure to change in bypass-exit airflow, 9.334 kilonewtons per square meter per kilogram per second.

(e) Engine-face static pressure. Ratio of change in pressure to change in bypass-exit airflow, 4.894 kilonewtons per square meter per kilogram per second.

Figure 22. - Concluded.

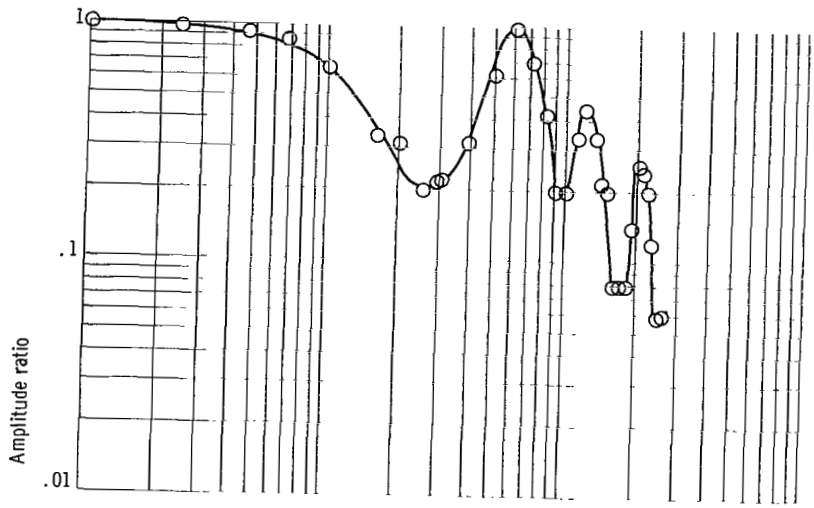

(a) Configuration II.

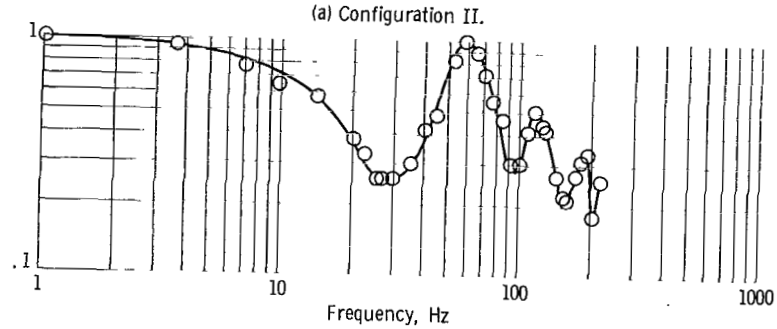

(b) Configuration I.

Figure 23. - Shock position dynamic response to unsymmetrical rotary valve internal disturbance by inlet unstart method; long cold pipe.

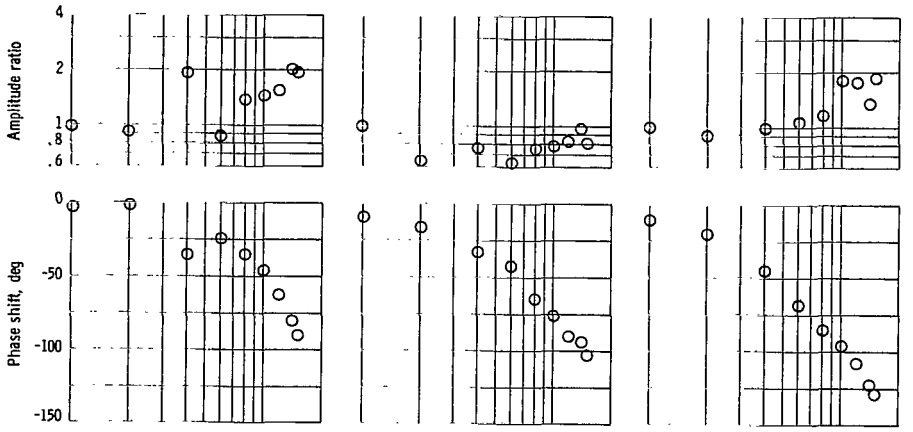

(a-1) Change in gust plate angle of attack, 0° to 1°; ratio of change in shock position to change in angle of attack, 1.3 centimeters per degree.

(a-2) Change in gust plate angle of attack, $\pm\frac{1}{2}°$; ratio of change in shock position to change in angle of attack, 1.3 centimeters per degree.

(a-3) Change in gust plate angle of attack, 0° to -1°; ratio of change in shock position to change in angle of attack, 0.8 centimeter per degree.

(a) Shock position.

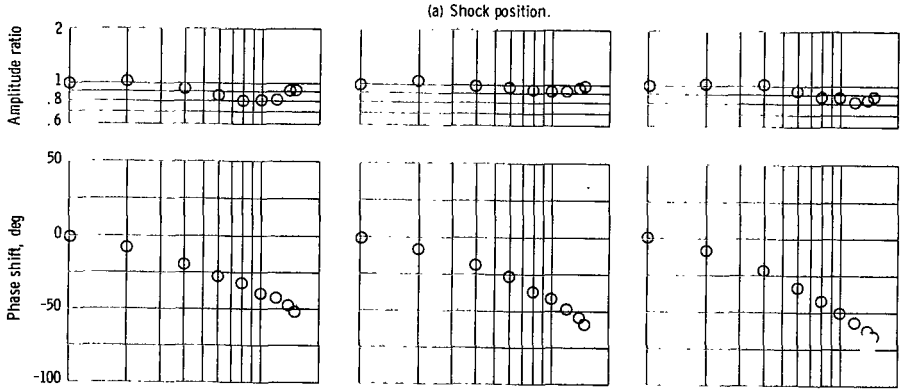

(b-1) Change in gust plate angle of attack, 0° to 1°; ratio of change in pressure to change in angle of attack, 1.53 kilonewtons per square meter per degree.

(b-2) Change in gust plate angle of attack, $\pm\frac{1}{2}°$; ratio of change in pressure to change in angle of attack, 2.37 kilonewtons per square meter per degree.

(b-3) Change in gust plate angle of attack, 0° to -1°; ratio of change in pressure to change in angle of attack, 1.08 kilonewtons per square meter per degree.

(b) Throat exit static pressure.

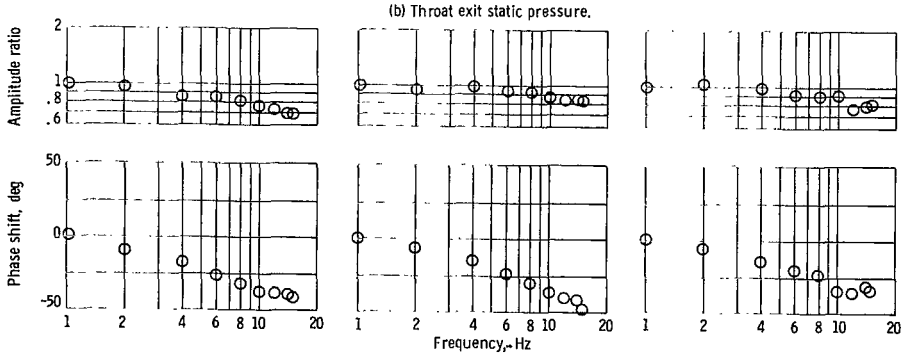

(c-1) Change in gust plate angle of attack, 0° to 1°; ratio of change in pressure to change in angle of attack, 1.32 kilonewtons per square meter per degree.

(c-2) Change in gust plate angle of attack, $\pm\frac{1}{2}°$; ratio of change in pressure to change in angle of attack, 2.18 kilonewtons per square meter per degree.

(c-3) Change in gust plate angle of attack, 0° to -1°; ratio of change in pressure to change in angle of attack, 0.794 kilonewton per square meter per degree.

(c) Static pressure before bypass cavity.

Figure 24. - Dynamic response to external disturbance. Inlet-engine: configuration II. Free-stream conditions: Mach number, 2.497; total pressure, 100.5 kilonewtons per square meter; total temperature, 342 K, ratio of specific heats, 1.400.

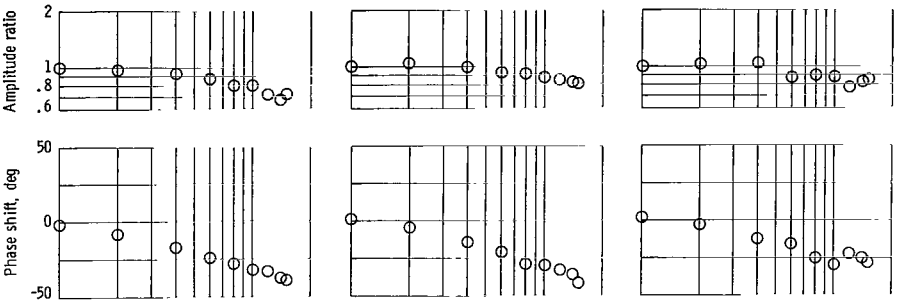

(d-1) Change in gust plate angle of attack, 0° to 1°; ratio of change in pressure to change in angle of attack, 1.197 kilonewtons per square meter per degree.

(d-2) Change in gust plate angle of attack, $\pm\frac{1}{2}^{\circ}$; ratio of change in pressure to change in angle ot attack, 2.155 kilonewtons per square meter per degree.

(d-3) Change in gust plate angle of attack, 0° to -1°; ratio of change in pressure to change in angle of attack, 6.36 kilonewtons per square meter per degree.

(d) Bypass cavity static pressure.

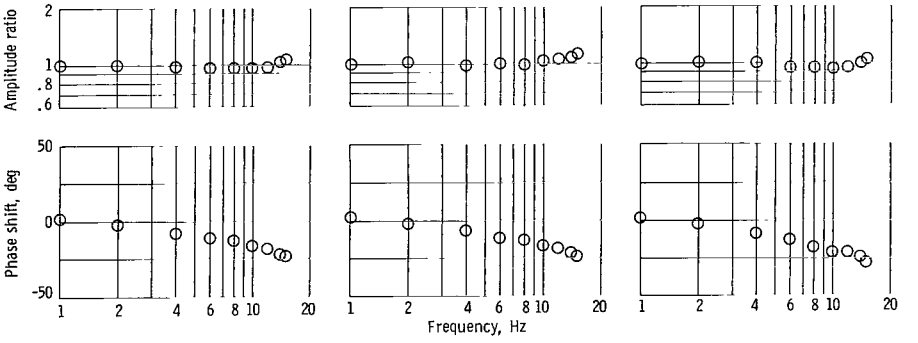

(e-1) Change in gust plate angle of attack, 0° to 1°; ratio of change in pressure to change in angle of attack, 1.407 kilonewtons per square meter per degree.

(e-2) Change in gust plate angle of attack, $\pm\frac{1}{2}^{\circ}$; ratio of change in pressure to change in angle of attack, 1.876 kilonewtons per square meter per degree.

(e-3) Change in gust plate angle of attack, 0° to -1°; ratio of change in pressure to change in angle of attack, 1.501 kilonewtons per square meter per degree.

(e) Engine face static pressure.

Figure 24. - Concluded.

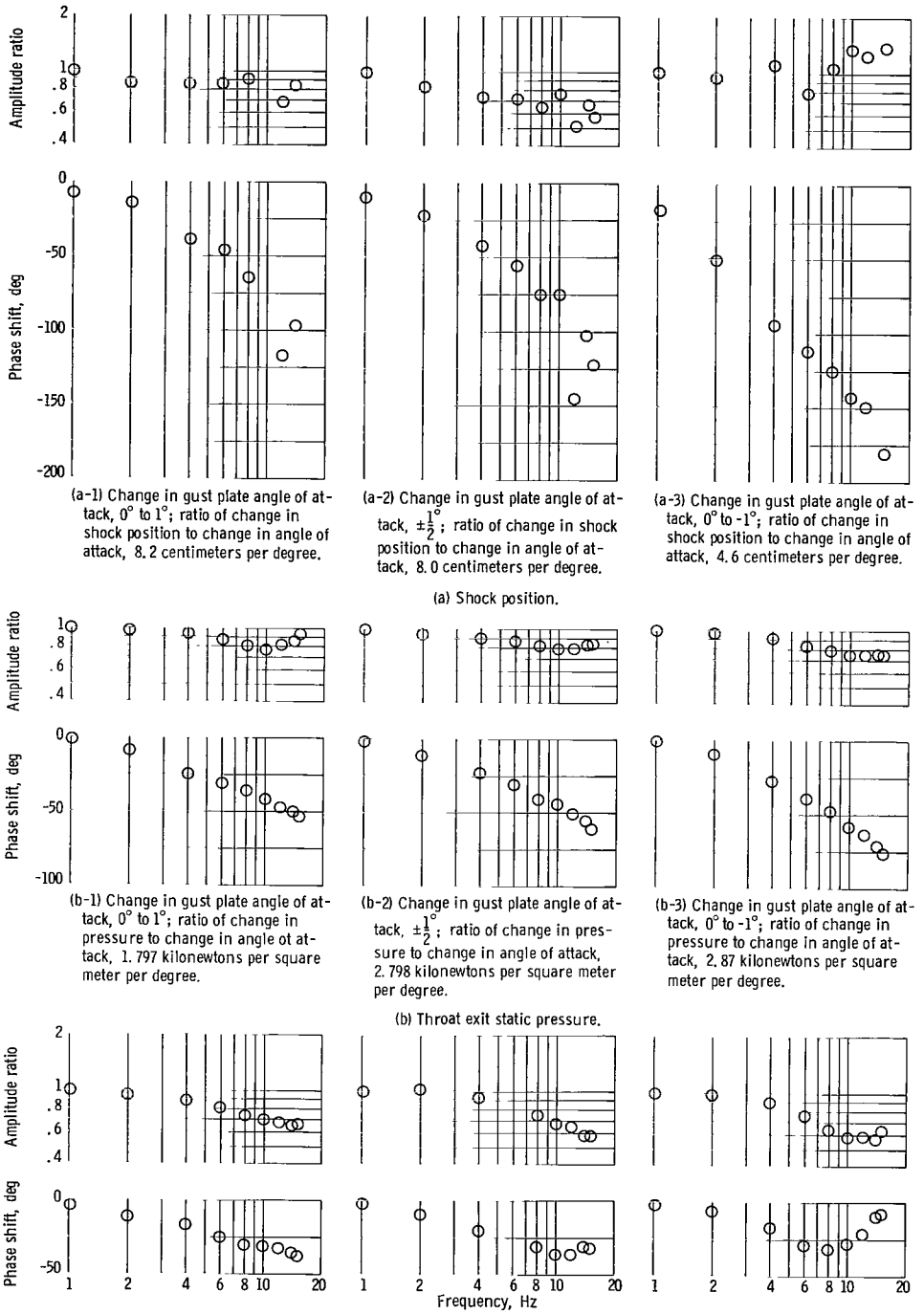

(a-1) Change in gust plate angle of attack, 0° to 1°; ratio of change in shock position to change in angle of attack, 8.2 centimeters per degree.

(a-2) Change in gust plate angle of attack, $\pm\frac{1}{2}$°; ratio of change in shock position to change in angle of attack, 8.0 centimeters per degree.

(a-3) Change in gust plate angle of attack, 0° to -1°; ratio of change in shock position to change in angle of attack, 4.6 centimeters per degree.

(a) Shock position.

(b-1) Change in gust plate angle of attack, 0° to 1°; ratio of change in pressure to change in angle ot attack, 1.797 kilonewtons per square meter per degree.

(b-2) Change in gust plate angle of attack, $\pm\frac{1}{2}$°; ratio of change in pressure to change in angle of attack, 2.798 kilonewtons per square meter per degree.

(b-3) Change in gust plate angle of attack, 0° to -1°; ratio of change in pressure to change in angle of attack, 2.87 kilonewtons per square meter per degree.

(b) Throat exit static pressure.

(c-1) Change in gust plate angle of attack, 0° to 1°; ratio of change in pressure to change in angle of attack, 1.74 kilonewtons per square meter per degree.

(c-2) Change in gust plate angle of attack, $\pm\frac{1}{2}$°; ratio of change in pressure to change in angle of attack, 1.854 kilonewtons per square meter per degree.

(c-3) Change in gust plate angle of attack, 0° to -1°; ratio of change in pressure to change in angle of attack, 1.629 kilonewtons per square meter per degree.

(c) Static pressure before bypass cavity.

Figure 25. - Dynamic response to external disturbance. Inlet engine; configuration I. Free-stream conditions: Mach number, 2.497; total pressure, 99.8 kilonewtons per square meter; total temperature, 342 K; ratio of specific heats, 1.400.

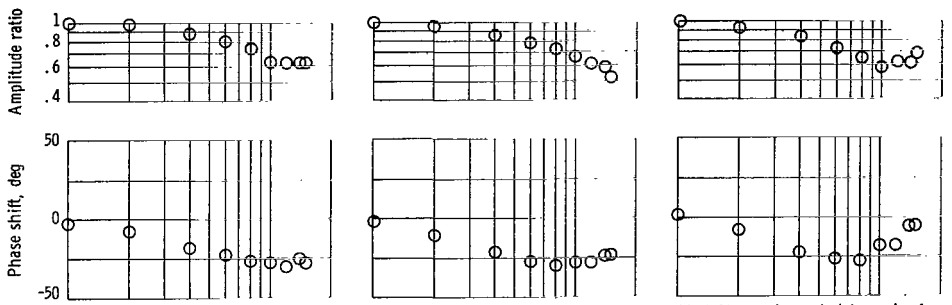

(d-1) Change in gust plate angle of attack, 0° to 1°; ratio of change in pressure to change in angle of attack, 1.606 kilonewtons per square meter per degree.

(d-2) Change in gust plate angle of attack, $\pm\frac{1}{2}^{\circ}$; ratio of change in pressure to change in angle of attack, 1.726 kilonewtons per square meter per degree.

(d-3) Change in gust plate angle of attack, 0° to -1°; ratio of change in pressure to change in angle of attack, 1.51 kilonewtons per square meter per degree.

(d) Bypass cavity static pressure.

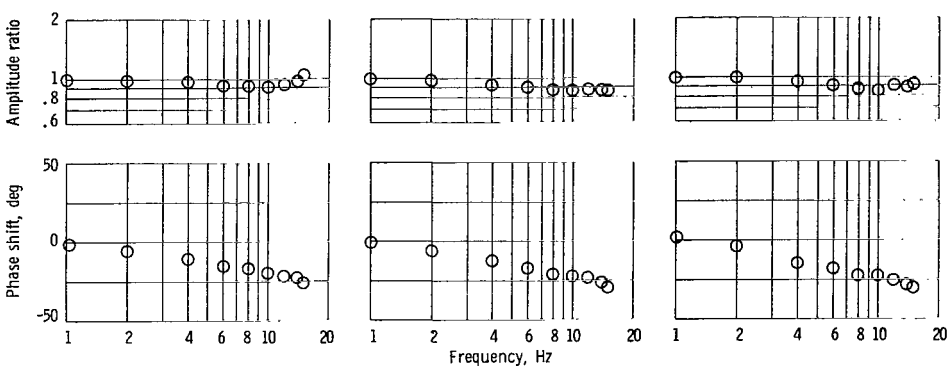

(e-1) Change in gust plate angle of attack, 0° to 1°; ratio of change in pressure to change in angle of attack, 1.702 kilonewtons per square meter per degree.

(e-2) Change in gust plate angle of attack, $\pm\frac{1}{2}^{\circ}$; ratio of change in pressure to change in angle of attack, 1.979 kilonewtons per square meter per degree.

(e-3) Change in gust plate angle of attack, 0° to -1°; ratio of change in pressure to change in angle of attack, 2.115 kilonewtons per square meter per degree.

(e) Engine face static pressure.

Figure 25. - Concluded.

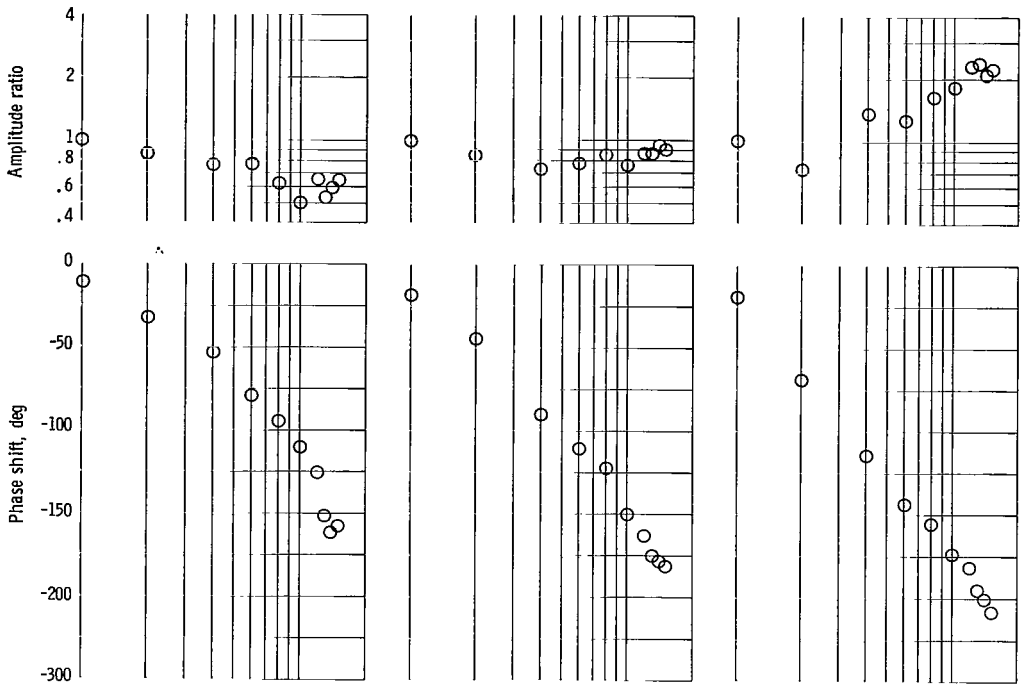

(a-1) Change in gust plate angle of attack, 0° to 1°; ratio of change in shock position to change in angle of attack, 8.8 centimeters per degree.

(a-2) Change in gust plate angle of attack, $\pm\frac{1}{2}°$; ratio of change in shock position to change in angle of attack, 7.7 centimeters per degree.

(a-3) Change in gust plate angle of attack, 0° to -1°; ratio of change in shock position to change in angle of attack, 4.7 centimeters per degree

(a) Shock position.

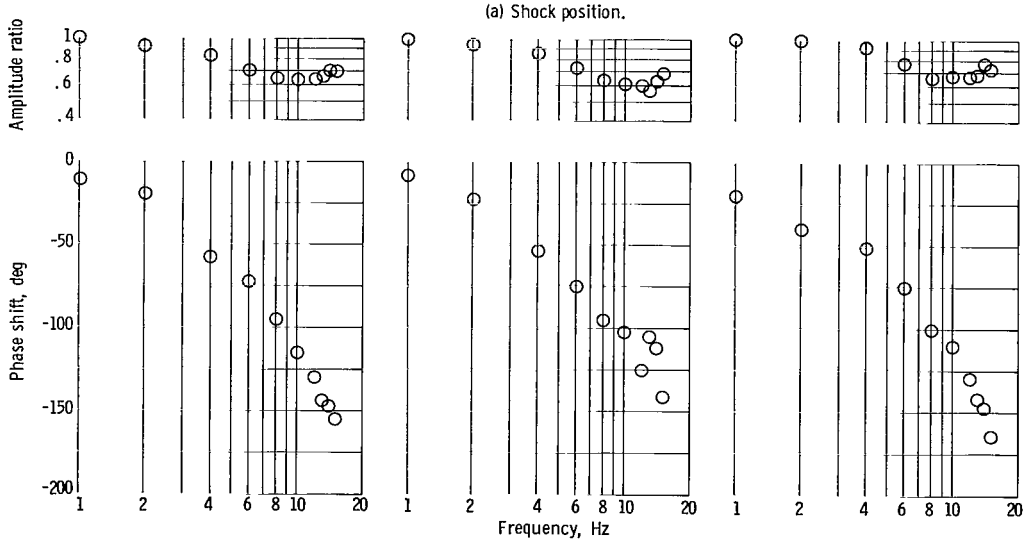

(b-1) Change in gust plate angle of attack, 0° to 1°; ratio of change in pressure to change in angle of attack, 2.208 kilonewtons per square meter per degree.

(b-2) Change in gust plate angle of attack, $\pm\frac{1}{2}°$; ratio of change in pressure to change in angle of attack, 2.872 kilonewtons per square meter per degree.

(b-3) Change in gust plate angle of attack, 0° to -1°; ratio of change in pressure to change in angle of attack, 3.257 kilonewtons per square meter per degree.

(b) Throat exit static pressure.

Figure 26. - Dynamic response to external disturbance. Long cold pipe; configuration I. Free-stream conditions: Mach number, 2.497; total pressure, 90.2 kilonewtons per square meter, total temperature, 316, K; ratio of specific heats, 1.400.

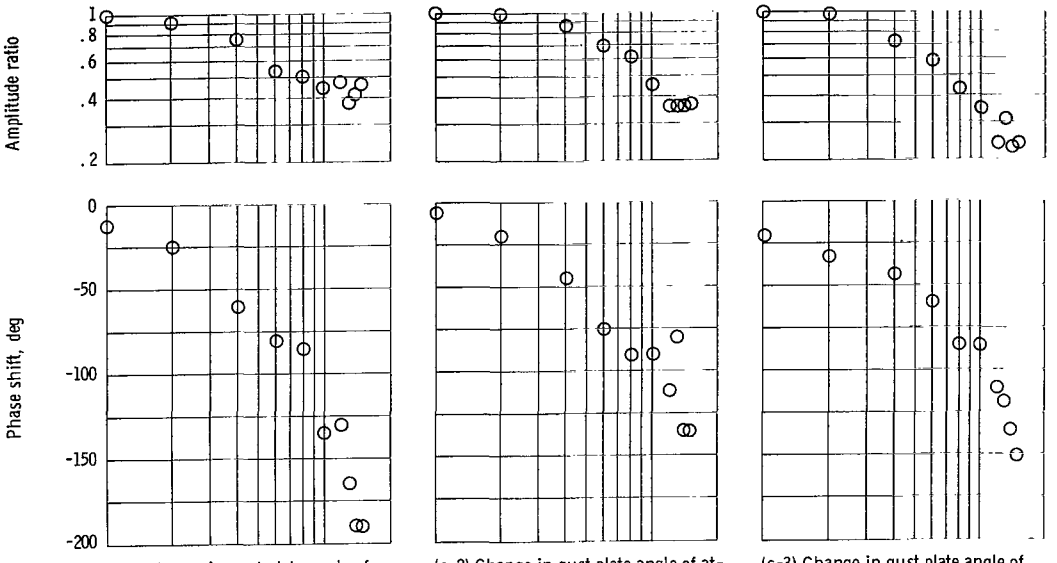

(c-1) Change in gust plate angle of attack, 0° to 1°; ratio of change in pressure to change in angle of attack, 1.702 kilonewtons per square meter per degree.

(c-2) Change in gust plate angle of attack, $\pm\frac{1}{2}^{\circ}$; ratio of change in pressure to change in angle of attack, 2.230 kilonewtons per square meter per degree.

(c-3) Change in gust plate angle of attack, 0° to -1°; ratio of change in pressure to change in angle of attack, 2.74 kilonewtons per square meter per degree.

(c) Bypass cavity static pressure.

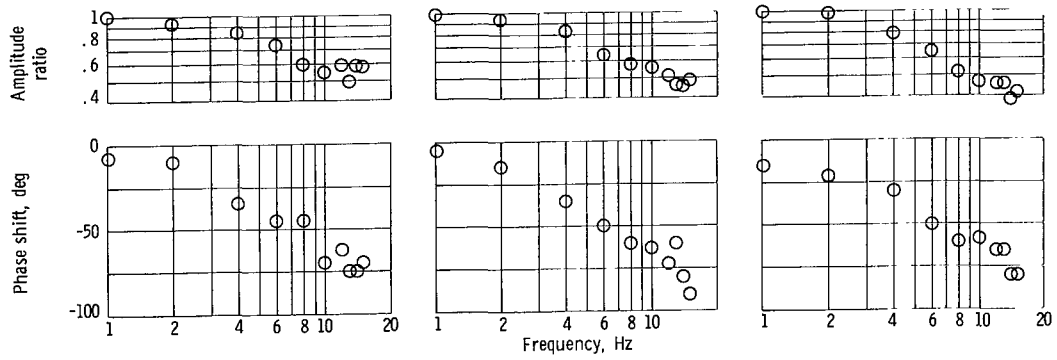

(d-1) Change in gust plate angle of attack, 0° to 1°; ratio of change in pressure to change in angle of attack, 1.78 kilonewtons per square meter per degree.

(d-2) Change in gust plate angle of attack, $\pm\frac{1}{2}^{\circ}$; ratio of change in pressure to change in angle of attack, 2.425 kilonewtons per square meter per degree.

(d-3) Change in gust plate angle of attack, 0° to -1°; ratio of change in pressure to change in angle of attack, 3.279 kilonewtons per square meter per degree.

(d) Engine face static pressure.

Figure 26. - Concluded.

NASA-Langley, 1969 — 28 E-4958

NATIONAL AERONAUTICS AND SPACE ADMINISTRATION
WASHINGTON, D. C. 20546

OFFICIAL BUSINESS

FIRST CLASS MAIL

POSTAGE AND FEES PAID
NATIONAL AERONAUTICS AND
RATION

POSTMASTER: If Undeliverable (Section 158 Postal Manual) Do Not Return

"The aeronautical and space activities of the United States shall be conducted so as to contribute . . . to the expansion of human knowledge of phenomena in the atmosphere and space. The Administration shall provide for the widest practicable and appropriate dissemination of information concerning its activities and the results thereof."

—NATIONAL AERONAUTICS AND SPACE ACT OF 1958

NASA SCIENTIFIC AND TECHNICAL PUBLICATIONS

TECHNICAL REPORTS: Scientific and technical information considered important, complete, and a lasting contribution to existing knowledge.

TECHNICAL NOTES: Information less broad in scope but nevertheless of importance as a contribution to existing knowledge.

TECHNICAL MEMORANDUMS: Information receiving limited distribution because of preliminary data, security classification, or other reasons.

CONTRACTOR REPORTS: Scientific and technical information generated under a NASA contract or grant and considered an important contribution to existing knowledge.

TECHNICAL TRANSLATIONS: Information published in a foreign language considered to merit NASA distribution in English.

SPECIAL PUBLICATIONS: Information derived from or of value to NASA activities. Publications include conference proceedings, monographs, data compilations, handbooks, sourcebooks, and special bibliographies.

TECHNOLOGY UTILIZATION PUBLICATIONS: Information on technology used by NASA that may be of particular interest in commercial and other non-aerospace applications. Publications include Tech Briefs, Technology Utilization Reports and Notes, and Technology Surveys.

Details on the availability of these publications may be obtained from:

SCIENTIFIC AND TECHNICAL INFORMATION DIVISION

NATIONAL AERONAUTICS AND SPACE ADMINISTRATION

Washington, D.C. 20546